

Metallicities and Radial Velocities of Five Open Clusters Including a New Candidate Member of the Monoceros Stream^{*}

Steven R. Warren¹ and Andrew A. Cole^{2,1}

¹*Department of Astronomy, 116 Church Street, S.E., Minneapolis, MN 55455; warren@astro.umn.edu*

²*School of Mathematics & Physics, University of Tasmania, Private Bag 37, Hobart, TAS 7001, Australia; andrew.cole@utas.edu.au*

3 November 2018

ABSTRACT

Near infrared spectra of 133 red giant stars from ten Galactic open clusters and two Galactic globular clusters spanning 2.2 dex in metallicity and 11 Gyr in age are presented. We combine this sample with ten clusters from Cole and collaborators to investigate the Ca II triplet line strengths and their relation to cluster metallicity and position along the red giant branch. We show that characterizing the stellar surface gravity using K_s band photometry (relative to the horizontal branch) taken from the Two Micron All-Sky Survey allows for metallicity measurements at least as precise as those derived using V or I band data. This has the great advantage that uniform photometry and reliable astrometry is available for a large number of clusters. Using K_s band photometry also reduces the effect of differential reddening within a given cluster. We find no significant evidence for age or metallicity effects to the linear Ca II triplet - metallicity relationship over the small range in magnitudes studied when homogeneous reference metallicities are used. We derive the first spectroscopic metallicity and new radial velocity estimates for five open clusters: Berkeley 81, Berkeley 99, IC 1311, King 2, and NGC 7044. King 2 has an anomalous radial velocity compared with the local disk population. We discuss the possibility that it is part of the Monoceros tidal stream.

Key words: techniques: spectroscopic – stars: abundances – stars: late-type – globular clusters: general – open clusters: individual (Berkeley 81, Berkeley 99, IC 1311, King 2, NGC 7044)

1 INTRODUCTION

The metallicities of star clusters and of multi-component stellar populations in galaxies are among their most important fundamental parameters. However, it is often difficult and/or time-consuming to reliably measure the metallicity or metallicity distribution of a population. This difficulty is reflected in the fact that for many open clusters in the Milky Way, the metallicity is still only known in an extremely vague sense, based on broadband photometry of the cluster main sequence. This state of affairs persists even though old open clusters are widely recognized as testbeds for stellar evolution theory and tracers of the age-metallicity relation and abundance gradient

in the Galaxy (e.g., Twarog, Ashman & Anthony-Twarog 1997; Friel et al. 2002; Bragaglia & Tosi 2006). Reliable spectroscopically-measured abundances, cheaply obtained, are vital to progress in studies of the kinematics and chemical evolution of clusters and galaxies.

Ideally, spectra of resolution $R \gtrsim 30,000$ and $S/N \gtrsim 100$ are used to provide a detailed element-by-element assay of the metallicity for multiple stars in each cluster. However, this is expensive in both telescope and analysis time, and has only been thoroughly carried out for a handful of the thousands of Milky Way clusters (e.g., Yong, Carney & Teixeira 2005; Carretta, Bragaglia & Gratton 2007; Jacobsen, Friel & Pilachowski 2007, and references therein). Spectroscopy of the near-infrared calcium triplet (CaT) in K giants emerged in the 1990s as a practical alternative for deriving the overall metal content of distant populations (Armandroff & Da Costa 1991), empirically calibrated on Galactic globular clusters (Rutledge et al. 1997b). Recently,

^{*} Based on observations made with the William Herschel Telescope operated on the island of La Palma by the Isaac Newton Group in the Spanish Observatorio del Roque de los Muchachos of the Instituto de Astrofísica de Canarias.

this technique has begun to be applied to open clusters, both as a path to confirming its applicability to the younger stars typical of dwarf irregular galaxies and the metal-rich stars characteristic of the M31 disk and bulge, and as a tool to explore open cluster metallicities in their own right (e.g., Cole et al. 2004; Carrera et al. 2007). A powerful application to the age-metallicity relation and abundance gradient of the star clusters of the Large Magellanic Cloud was demonstrated by Grocholski et al. (2006). The applicability of the CaT technique to composite stellar populations with a diverse mixture of ages, metallicities, and alpha-element enhancements was reconfirmed by Battaglia et al. (2008).

The aim of this paper is twofold: to increase the flexibility and applicability of the CaT technique by extending the line-strength-magnitude-metallicity relation to near-infrared passbands, and to provide the first spectroscopic metallicity and radial velocity estimates of several distant, understudied open clusters. The advantage of deriving CaT metallicities using K_s -band photometry is that surveys such as the Two Micron All-Sky Survey (2MASS; Skrutskie et al. 2006) make it possible to apply the technique to nearly any star accessible to CaT spectroscopy from a 4-metre class telescope. In the case of 2MASS, the survey astrometry is also precise enough to accurately place spectrograph fibres or slitlets, making it a one-stop shop for lead-up to a multi-object spectroscopy observing campaign.

We discuss our approach, observations, reductions, and analysis in §2. We show that the K_s magnitude of the red clump/horizontal branch is at least as precise a surface gravity proxy as various techniques in the literature that use the V or I bands. The metallicities of seventeen previously studied globular and open clusters are found to be in good agreement with high-dispersion $[\text{Fe}/\text{H}]$ values. Using these clusters as a calibration sample, we present new abundance and radial velocity measurements for five understudied clusters in §3. In most cases the cluster metallicities are consistent with inferences from colour-magnitude diagrams (CMDs), and the kinematics and metallicities are suggestive of thick disk membership. However, the cluster King 2 has a strongly discrepant radial velocity compared to tracers of the disk; we discuss the possibility that it may be a member of the Monoceros stream in §4. We conclude with discussion of our results in §5.

2 OBSERVATIONS AND DATA REDUCTION

The CaT has risen to a pre-eminent position among metallicity indicators for faint red giants. The large-scale study of globular clusters in Rutledge et al. (1997a) and Rutledge et al. (1997b) led to the work of Cole et al. (2004), Carrera et al. (2007), and Battaglia et al. (2008) to systematize and optimize the precision of the CaT-based methods. The CaT is quite sensitive to surface gravity as well as metallicity (e.g., Jones, Alloin & Jones 1984; Jørgensen, Carlsson & Johnson 1992), and so a proxy for this quantity, usually a photometric measure for practical reasons, is used to obtain a metallicity from the CaT line width. The main difference between various groups and authors is in their choice of passband and reference level for the gravity proxy. The most popular choice, dating to the work of Rutledge et al. (1997a), is the V magnitude dis-

tance above the horizontal branch, but the I band absolute magnitude has also been advocated (Carrera et al. 2007). To extend the previous work of Cole et al. (2004) and measure abundances and radial velocities for some understudied clusters, we observed a sample of ten Galactic open clusters and two Galactic globular clusters with the multifibre spectrograph at the William Herschel Telescope on La Palma. In selecting targets, we found it difficult to obtain V and I photometry across the large spectrographic fields, even though most clusters have been well-surveyed in their central regions. We realized that the 2MASS catalog was the only homogeneous dataset to completely cover all of the clusters in our sample. To preserve as much homogeneity as possible, we investigate the CaT - metallicity relationship using 2MASS K_s photometry.

We observed a sample of ten Galactic open clusters and two Galactic globular clusters with the multifibre spectrograph at the William Herschel Telescope on La Palma. Five of the ten open clusters (NGC 6791, NGC 6819, NGC 6939, NGC 7142, and NGC 7789) and both of the globular clusters (M15 and M71) have been extensively studied. Each has had metallicity determinations from high- or medium-dispersion spectroscopy and model atmosphere analysis, although the measurements are diverse in their choices of atmospheres, temperature and surface gravity determinations, so the $[\text{Fe}/\text{H}]$ values are strongly inhomogeneous. We discuss the choice of reference metallicities below. Individual cluster members that have previously published radial velocities are also used as cross-correlation templates in our radial velocity measurements.

In order to reasonably sample the line-strength-magnitude-metallicity parameter space, we combined our sample with the ten calibration clusters of Cole et al. (2004). 2MASS K_s photometry was found for all but three stars in their sample (NGC 2298: SH156 and SH172 (T. Smecker-Hane, unpublished); NGC 104: L5528 (Lee 1977)). Including measurements taken from different sources can introduce hidden systematic effects if proper care is not taken. Nonetheless these seventeen clusters serve as a calibration sample from which we derive our relationship between CaT equivalent width, K_s magnitude, and metallicity. We test our ability to combine the samples below. The pertinent cluster parameters are summarized in Table 1.

2.1 Understudied Clusters

We applied our calibration to five clusters for which we could find no published spectroscopic metallicity measurement. Apart from northern hemisphere early summer visibility, our only requirement was for the clusters to contain at least 30 red giants¹. Our understudied cluster sample consists of Berkeley 81, Berkeley 99, IC 1311, King 2, and NGC 7044. The selected clusters were taken to be representative of the surviving old ($\geq 10^9$ yr) open clusters of the Milky Way, typified by, e.g., M67, NGC 2141, or the well-studied clusters of our sample. Some references to IC 1311 make it younger than 10^9 yr (e.g., Carraro & Chiosi 1994 and the WEBDA database value), but the CMD morphology suggests it is

¹ as per the listing at the WEBDA database, <http://www.univie.ac.at/webda/>

comparable in age to Be 81 or NGC 7044. The useful cluster parameters are given in Table 2.

One of the biggest uncertainties in determining a proper CaT versus metallicity relationship is the lack of a universally-accepted, high-dispersion fiducial sample of globular and open clusters. Large databases of high-dispersion metallicities have been created for globular clusters (e.g., Carretta & Gratton 1997; Kraft & Ivans 2003), and medium-resolution metallicities (Friel et al. 2002) or medium-band photometry (Twarog, Ashman & Anthony-Twarog 1997) for open clusters, but no large studies combining globular and open clusters on a homogeneous basis have been made as of yet (as noted by Cole et al. 2004; Carrera et al. 2007). Therefore the metallicities we determine are always referred back to a particular metallicity scale from the literature.

2.2 The Red Giant Star Sample

Red giant branch (RGB) stars were chosen from 2MASS J and K_s photometry in the regions of the selected clusters. (K_s , $J - K_s$) CMDs were created for square-degree areas centered on each cluster, and targets were selected from the cluster RGB locus down to and including the RGB clump (RC). The cluster radii were initially chosen to match the values in Lyngå (1987), although they were varied slightly to optimize the contrast between the cluster and the field in the CMD in some cases.

We tried to sample as wide a range of magnitude as possible in each cluster in order to accurately model the influence of surface gravity on the CaT equivalent widths. The spectrograph fibres are assigned according to an optimization algorithm that responds to user-supplied weightings for each star in the target file. The weightings are required because not every desired target can be observed in a single configuration due to the requirement that fibres not collide or bend at sharp angles. We assigned high weights to stars within the adopted cluster radii and very low weights to those outside; this was necessary because configurations with a high central concentration of targets are extremely susceptible to fibre collisions and tend to be avoided by the software. Because the RGB luminosity function is steeply decreasing with brighter magnitude, we weighted bright stars more heavily than stars near the RC; we expected that this would prevent the bright stars necessary to define our surface gravity correction from being excluded, and that an adequate sample of fainter stars near the RC would be filled in between the bright star targets with relative ease. This procedure appears to have succeeded for all clusters but Be 81, where a too-broad initial colour selection, poor tuning of the weighting algorithm and bad luck produced a situation where cluster membership remained ambiguous even considering the radial velocity information (section 3.1).

The central Be 81 problem is a lack of bright RGB stars, but this is an issue to varying degrees for nearly all open clusters (e.g., Cannon 1970). Additionally, the brightest, coolest stars are often contaminated by titanium oxide bands in the spectral region of interest, making them unusable for the CaT method. M stars so identified are noted in the figures for each cluster. In most cases, the cluster RGB sequences were not unambiguously distinct from the surrounding field, and the samples were cleaned after observation according to

radial velocity and position relative to the cluster center (see below). Because the field of view of the multifibre spectrograph is far larger than the sizes of the clusters, a large number of stars that were expected to be field stars were measured in order to solidly establish values of the foreground/background radial velocity as an aid to membership distinctions.

2.2.1 Defining the Red Clump K_s Magnitudes

It was necessary to define the mean K_s magnitude of the cluster red clumps (horizontal branches in the case of the globular clusters) so that the height of each target star above the clump could be defined. Each of the open clusters had previous red clump magnitude determinations from Cole & Weinberg (2001). The 2MASS point source catalog (K_s , $J - K_s$) CMDs for one square degree regions centered around each cluster were examined, and the radius was gradually reduced until further contraction began to exclude red clump stars without reducing the extent of the clump in K_s or $J - K_s$. The final selection regions ranged from $1'.8$ (IC 1311) to $12'$ (NGC 7789); these radii are not identical with cluster radii in the literature (e.g., Sagar & Griffiths 1998), but are roughly similar, and in all cases yielded a well-defined red clump. The same procedure was followed for the globular clusters, except for M15 and NGC 4590, for which the horizontal branch was close enough to the limit of the 2MASS photometry that an accurate K_s magnitude could not be found. In these two clusters, the appropriate values were taken from Ferraro et al. (2000). The horizontal branch is not horizontal in the (K_s , $J - K_s$) colour space; for clusters with an extended HB, we took the value of K_s at the RR Lyrae instability strip as the reference level. The values of $K_{s,RC}$ for previously observed and understudied clusters are found in Tables 1 and 2, respectively.

The exact sample selection to define $K_{s,RC}$ does not strongly influence our results in any case. Independent checks on our derived $K_{s,RC}$ values can be found in Grocholski & Sarajedini (2002) (GS02) and van Helshoecht & Groenewegen (2007) (vHG07), who each determined $K_{s,RC}$ for open cluster samples for use as a distance indicator. We have five clusters in common with GS02: NGC 6791, NGC 6819, and (from Cole et al. 2004) M67, Be 39, and 47 Tuc. The mean difference (us–GS02) is -0.008 mag, and the largest difference is -0.04 ± 0.11 mag, for M67. The same clusters plus NGC 7789 and Melotte 66 were included in the sample of vHG07; here we find a larger difference, with (us–vHG07) = -0.05 mag, ranging from -0.03 to -0.08 . Shifts this small are entirely insignificant to our derived metallicities. Even for Be 81, where just a few red clump stars within a 3.6 radius ($\sim 33\%$ larger than the cluster radius from Sagar & Griffiths (1998)) are distributed in a near-vertical feature, the adopted error of ± 0.4 mag on $K_{s,RC}$ only contributes ± 0.06 to the error budget for $[\text{Fe}/\text{H}]$ (see below).

2.3 Data Acquisition and Reduction

The data were obtained on 27–28 June, 2004 at the 4.2m William Herschel Telescope at La Palma, Spain. We used the WYFFOS wide field fibre optical spectrograph, fed by

the AF2 fibre-positioning system that allows simultaneous measurement of up to 150 objects over an un-vignetted 40' diameter field of view through its 1"6 diameter fibres. We used the low-order 'echelle' grating in 3rd order with $\lambda_{cen} = 8701 \text{ \AA}$ and the GG495 order-blocking filter, yielding a spectral coverage of 570 \AA and a spectral resolution of $\approx 0.15 \text{ \AA/pix}$. The weather was clear but the seeing was moderate to poor, resulting in some light loss from the fibres. Typical exposure times ranged from 480–900 seconds. Offset sky exposures were taken after each science frame, with a typical offset of 2 arcseconds. Neon arcclamp and screen flat exposures were also taken subsequent to each image to allow flatfielding and wavelength calibration.

Data reduction was performed under IRAF using Pierre Leisy's instrument-specific reduction scripts². The reduction package corrects the CCD bias using zero frames and an overscan region, and trims the image. The individual fibres are automatically found, traced along the CCD, and extracted using standard flatfield and wavelength calibration procedures.

Examination of the residuals from the sky subtraction process showed that the night-sky emission lines of OH (Osterbrock & Martel 1992) were frequently either under- or over-subtracted during the calibration. Therefore we developed an iterative process to optimize the sky subtraction for each fibre in each image. We processed the offset sky fields for each cluster using the same reduction script parameters as used for the clusters themselves, and matched each fibre in the offset sky to the corresponding fibre in the science exposure. Each sky spectrum was scaled by a wavelength-independent factor of order unity and subtracted from the matching object spectrum, leaving a residual spectrum whose rms scatter was measured. The scaling factor was then adjusted iteratively until the rms reached a minimum value.

The sky-subtracted exposures were then continuum normalized using a low-order polynomial fit to spectral regions excluding areas of strong telluric water vapor absorption. Figure 1 shows the raw, sky, and reduced spectra for a typical target. Except in a few cases, the S/N/pixel in our final, extracted spectra was $\gtrsim 20$.

2.4 Radial Velocities

Radial velocities are important in determining membership probabilities as well as estimating the expected line centers of the CaT for use in the equivalent width measurements. We derived relative radial velocities of our sample stars by cross-correlating their spectra with reference stars within our sample (Tonry & Davis 1979). The reference stars chosen have previously derived radial velocities taken from the literature. We chose three stars from M15 (Soderberg et al. 1999), three from NGC 7789 (Gim et al. 1998), and one from NGC 6819 (Friel & Janes 1993). The IRAF FXCOR task was then used to perform the cross-correlation with each of the seven reference spectra. Final radial velocities were then derived by taking the weighted average of the results from each reference spectrum. The weighted average included the errors in the correlation and correlation peak height. Stars

whose radial velocities differed greatly from the cluster mean radial velocity were removed from consideration as well as those stars whose distances from the cluster center were beyond visually inspected cluster bounds. The velocities and standard errors are given in Table 4 and the velocity cuts are shown in Figure 2.

2.5 Equivalent Width Measurements

Methods for deriving the equivalent widths of the CaT lines have been previously discussed in Cole et al. (2004). Cole et al. showed that a sum of a Gaussian and a Lorentzian produced an empirical function that fit the line profiles more accurately over a wide range of line strengths than a Gaussian (e.g. Armandroff & Da Costa 1991) alone. The Gaussian profile, while having an acceptable fit for weak lines, underestimates the equivalent widths for strong lines by failing to incorporate the broadened CaT wings. The same is true for the Moffat function used by Rutledge et al. as shown by Pont et al. (2004). Based on this, we have used the sum of a Gaussian and Lorentzian to define our empirical function and integrated the result to calculate the equivalent width of the CaT lines. We measured the equivalent widths using the `ew` program (Cole et al. 2004) to fit the continuum around each line with a linear function and the lines with a Gaussian+Lorentzian that are forced to have the same central wavelength. Bad pixels and residuals from cosmic ray removal are rejected from the line and continuum fits using an iterative sigma-clipping method, and the residuals to the fits are visually inspected. The line and continuum bandpasses are listed in Table 3.

The equivalent width of a spectral line can be strongly affected by other atomic and molecular line opacities that alter the continuum level around the features of interest. Two important contaminants around the calcium triplet are titanium oxide (TiO) and cyanogen (CN) bands. TiO can suppress the continuum between $8430 \text{ \AA} \lesssim \lambda \lesssim 8550 \text{ \AA}$, making the CaT lines appear weaker than they actually are. TiO bands become problematic for giants cooler than late K-type, and are especially troublesome at high metallicity (e.g., NGC 6791). CN bands can have a similar depressing effect on the CaT lines, but they are more symptomatic of stellar nucleosynthesis and dredge-up processes than of cool temperatures. We have carefully inspected the spectrum of each star and rejected from further analysis the targets that showed the signatures of TiO or CN bands.

2.5.1 The CaT Index

The CaT index (ΣW ; Armandroff & Da Costa 1991) is taken as a linear combination of the pseudo-equivalent widths of the three Ca II lines ($\lambda\lambda = 8498.02, 8542.09, 8662.14 \text{ \AA}$). Rutledge et al. (1997a) explored the impact of including or excluding the weakest line and various weighting schemes as a function of signal-to-noise. Studies with poor spectral resolution and/or low S/N usually form ΣW excluding the weak 8498 \AA line (Suntzeff et al. 1993; Cole et al. 2000; Battaglia et al. 2008), while others have used an unweighted sum of all three lines (Olszewski et al. 1991; Cole et al. 2004; Carrera et al. 2007). Given the high quality of our spectra (S/N/pixel $\gtrsim 20$) we have adopted a straight sum of the three individual lines:

² <http://www.ing.iac.es/Astronomy/instruments/af2>

$$\Sigma W = W_{8498} + W_{8542} + W_{8662}.$$

The exact value of ΣW will vary from study to study because there is some freedom in choosing the continuum level to which the equivalent width values are referred. The values should fall within the uncertainties reported for ΣW if the errorbars are properly estimated.

Armandroff & Da Costa (1991) introduced a ‘reduced’ equivalent width parameter, W' , used to effectively remove the surface gravity and effective temperature dependences of the line strength, leaving only the metallicity dependence. Because red giants lie along a narrow sequence in the luminosity (surface gravity) vs. temperature plane, T_{eff} and $\log(g)$ are correlated with each other and their influence on ΣW can be calibrated out using a single observable. Colour and absolute magnitude have both been used in the past to create the index W' , but the most robust method in the presence of distance and reddening uncertainties is to use an expression relating the magnitude of the target star to the mean magnitude of the horizontal branch (or red clump) of its parent population:

$$W' = \Sigma W + \beta(\mathfrak{M} - \mathfrak{M}_{HB}),$$

where β depends on the definition of ΣW and on the band-pass \mathfrak{M} used in the comparison. Since we assume that each star in a given cluster has the same metallicity and thus the same W' value, the error on W' , $\sigma_{W'}$, depends on the standard deviation of the individual stars’ W' values about the mean cluster value as well as the number of stars, N , used in each cluster.

$$\sigma_{W'} = \frac{\sigma}{\sqrt{N}}$$

Because much of the opacity in the very strong Ca II lines lies in the wings, the measured increase of line strength with decreasing surface gravity is to some degree dependent on the functional form adopted to measure the lines, and on the S/N of the data. Therefore the standard best practice is for calibration clusters to be observed, providing a constant metallicity sample from which appropriate β values can be derived. Individual studies have found no dependence of β on metallicity or age (Rutledge et al. 1997a), but studies including open as well as globular clusters tend to find slightly higher β values (e.g., Cole et al. 2004). If stars below the horizontal branch or above the tip of the red giant branch are included, the linear relation between ΣW , $(\mathfrak{M} - \mathfrak{M}_{HB})$, and $[\text{Fe}/\text{H}]$ breaks down, and an $(\mathfrak{M} - \mathfrak{M}_{HB})^2$ term must be introduced (Carrera et al. 2007).

Previously, Johnson V and Cousins I have been the most commonly used magnitudes for the formation of W' . Typical values are $\beta_V \approx 0.7$ (e.g., Rutledge et al. 1997b, Cole et al. 2004). However, in many open clusters only a small region of the cluster center has published photometry, and in some cases that photometry predates the CCD era and so would be difficult to replicate consistently. However, the Two Micron All-Sky Survey has provided near-infrared JHK_s magnitudes on a uniform scale over the entire sky down to $K_s \approx 14$, below the red clump/horizontal branch level for many open clusters. This provides the tantalizing prospect of using the near-infrared photometry to form W' , obviating

the need to search through a large number of inhomogeneous studies to accumulate the necessary VI photometry.

Using 2MASS data instead of optical data also has many advantages. K_s is less sensitive to reddening by dust than V or I , therefore any intra-cluster reddening dependence in W' is reduced. Also, Carpenter (2001) derived transformation equations for many infrared filter sets such that their JHK_s colours can be placed on the 2MASS system. This gives a unique opportunity to maintain homogeneity in future studies.

2.6 W' and Metallicity

Typically, a linear relationship has been established between W' and $[\text{Fe}/\text{H}]$, but this depends crucially on the adopted metallicities of the calibration sample (see Cole et al. 2004 and references within). A linear relation between W' and $[\text{Fe}/\text{H}]$ has been called into question for metallicities on the widely-used Zinn & West (1984) scale as well as high-dispersion scales based on measurements of ionised rather than neutral iron (Kraft & Ivans 2003). Adopting metallicities from different sources will change the derived slope and intercept values. Higher order terms in the W' vs. $[\text{Fe}/\text{H}]$ relationship (Carretta et al. 2001; Cole et al. 2004; Carrera et al. 2007) may then be artificially introduced (see §2.8). With these issues in mind, we have decided to use the metallicities defined by Carretta & Gratton (1997) for the globular clusters and Friel et al. (2002) for the open clusters. Our best hope is to try and remain consistent throughout our analysis.

2.7 Combining the Two Data Sets

Before we can combine our cluster sample with that of Cole et al. (2004) we must first test if they are compatible with each other. One way to do this is to derive the W' vs. $[\text{Fe}/\text{H}]$ relationship for each sample individually and compare the results. Systematic effects from instrumental and reduction differences can introduce non-linearities if the samples are incompatible.

In order to derive β for an individual cluster, we used 2MASS $K_s - K_{s,RC}$ magnitudes for each star plotted against ΣW . The slope of the best fit line, weighted by errors in ΣW , was computed for each calibration cluster. The mean slope value, β_{K_s} , weighted by the errors in the slopes, was then calculated. By using the 2MASS K_s magnitudes we derive a value of $\beta_{K_s} = 0.45 \pm 0.03$ for our sample and $\beta_{K_s} = 0.49 \pm 0.02$ for the Cole et al. (2004) sample.

We then derived the average W' value for each cluster and plotted them against the reference metallicities given in Table 1. We then fit each cluster sample with a line weighted by the metallicity errors (see Figure 3). The equations of the best line fits are

$$[\text{Fe}/\text{H}] = (-2.746 \pm 0.224) + (0.330 \pm 0.029)W'$$

for our sample and

$$[\text{Fe}/\text{H}] = (-2.754 \pm 0.076) + (0.332 \pm 0.012)W'$$

for the Cole et al. (2004) sample. The two lines are statistically similar and show that the two samples are indeed compatible. Any systematic effects between the samples are small and cannot be characterized here.

We can now move forward and combine the two samples and rederive β_{K_s} for the entire data set. Using all seventeen calibration clusters we derive a value of $\beta_{K_s} = 0.48 \pm 0.01$. Figures 4 and 5 show the best fit line with this slope through each of the calibration clusters.

With this β_{K_s} value, we then derived the final average W' value for each cluster and plotted them against the reference metallicity values given in Table 1. Figure 6 shows our best fit line to the data points with our adopted metallicities and derived W' values. The equation of the fit is

$$[Fe/H] = (-2.738 \pm 0.063) + (0.330 \pm 0.009)W'$$

which gives consistent predictions with what was derived by Cole et al. (2004) (see Table 7). Adding a second order term (W'^2) does not significantly improve the fit.

In order to evaluate our ability to estimate a cluster's metallicity, a check of our predicted $[Fe/H]$ value versus the true value is needed. The lower panel of Figure 6 shows $\Delta[Fe/H]$ vs. W' for each of the calibration clusters. The residual about the mean is -0.011 with a standard deviation, σ_{scat} , of 0.07. The scatter is expected given the scatter in W' and the reported errors on reference metallicity, and there are no obvious trends with cluster age or mean $K_s - K_{s,RC}$. Final errors on the $[Fe/H]$ predictions depend on the slope of the derived $[Fe/H]$ line ($m_{[Fe/H]}$), the error on W' ($\sigma_{W'}$), and σ_{scat} .

$$\sigma_{[Fe/H]} = \sqrt{(m_{[Fe/H]} * \sigma_{W'})^2 + \sigma_{scat}^2}$$

Tables 6 and 7 give our W' , predicted $[Fe/H]$, and reference $[Fe/H]$ values. Table 6 also gives our derived average cluster radial velocities and literature radial velocities values for our cluster sample. The derived cluster radial velocities are statistically similar to the literature values.

2.8 Different Metallicity Scales

If we choose reference metallicities from multiple sources we lose homogeneity in the most crucial part of the calibration procedure. As noted before, no studies have produced high-dispersion metallicities for all of our calibration clusters, so the final metallicity values are always referred back to the adopted scales. As an example to the sensitivity of the metallicity scale on the derived $[Fe/H]$ vs. W' calibration, we chose metallicity values derived from high-dispersion spectroscopy measurements made by different authors. We took our derived W' values for each cluster and plotted them against the reference metallicities listed in Table 8. Berkeley 39 currently has no high-dispersion metallicity estimates, so it was left out of this calibration. Table 8 and Figure 7 give the results of the fits.

The linear fit in the top panel of Figure 7 has an equation of

$$[Fe/H] = (-3.031 \pm 0.118) + (0.389 \pm 0.017)W'$$

with the residuals to the fit shown in the middle panel ($\sigma_{scat} = 0.13$). The quadratic fit results in

$$[Fe/H] = (-2.501 \pm 0.081) + (0.126 \pm 0.045)W' + (0.025 \pm 0.004)W'^2.$$

The residuals to the quadratic fit are shown in the bottom panel ($\sigma_{scat} = 0.10$). Neither fit perfectly reproduces the reference metallicities over the entire range if our W' errors and the quoted errorbars on the cluster metallicities

are realistic measures of the uncertainty. Neither fit appears significantly better than the other, and the significance of any putative improvement would be entirely dependent on the exact metallicity chosen for each calibration cluster and the adopted metallicity uncertainties; i.e., the variation in metallicity between disparate authors is usually larger than the quoted errorbars. This underscores the need for a uniform high-dispersion metallicity scale spanning clusters with a wide range of metallicities. For the remainder of this paper we will report the metallicities of our understudied clusters on the linear scale based on the combined Carretta-Gratton and Friel et al. samples, but future workers may recalibrate our reported W' values to any desired scale as new information becomes available.

3 RESULTS: NEW CLUSTER VELOCITIES AND METALLICITIES

The results for our calibration clusters show that the reduced equivalent width of the CaT obtained using 2MASS K_s magnitudes can reproduce the $[Fe/H]$ measurements obtained from high- and medium-dispersion spectroscopy and CaT measurements plus visible-light bandpasses. Therefore we can proceed with some confidence to derive metallicity estimates for previously understudied clusters. Prior to this study, very little was known about their metallicities and their radial velocities appeared to be unknown. Each of these clusters has at least one broadband CCD-based CMD in the literature, but medium-band photometry (e.g., DDO or Strömgen system) could not be found.

As with the calibration clusters, we plotted derived radial velocities versus distance from the cluster center in order to select potential cluster members. We can also use the 2MASS (K_s , $J - K_s$) colour-magnitude diagrams to check if the stars are in the expected RGB sequence of the cluster. Figures 9, 10, 11, 12, and 13 show the uncleaned 2MASS (K_s , $J - K_s$) CMDs. The CMDs include all of the point sources in the 2MASS field of view within a radius of the cluster center determined by the largest distance in the red giant star sample for each cluster. As a quick reference, the filled circles highlight the accepted star locations in each cluster while the open symbols are those stars rejected from our analysis. Refer to the figure captions for more explanation. Figure 8 shows radial velocity vs distance from cluster center. Again, stars that have been kept for further analysis are plotted as filled circles and open symbols are stars that have been excluded from further analysis.

Once our star sample has been defined we can use it to derive cluster parameters. Figure 14 is a plot of ΣW versus $K_s - K_{s,RC}$ for the accepted stars in each cluster. As in Figure 4, the best fit line has a forced slope equal to our derived β_{K_s} . The data points follow the linear relation found previously. With this information we can then compute W' and use this to derive $[Fe/H]$ for each cluster. Table 9 gives the derived W' , $[Fe/H]$, and radial velocity values for each of the understudied clusters.

3.1 Berkeley 81

The cluster sequence for Be 81 was the most difficult of the five new clusters to pick out, although most of the observed

spectra for the Be 81 sample were of good quality and only one spectrum showed contamination by TiO bands. With a large sample of stars, we would expect a grouping of stars with similar radial velocities about the cluster mean in a radial velocity versus radial distance plot; however, with the small number of stars in our sample, the large spread in radial velocities (see Figure 8) along the cluster line of sight made selecting the stars used for further analysis non-trivial. Just outside the adopted radius from section 2.2, the spread of radial velocities is $\approx 100 \text{ km s}^{-1}$. However, the 8 stars interior to the cutoff also show a large range of radial velocities, and the tendency to concentrate around $\approx 0 \pm 20 \text{ km s}^{-1}$ is not strong, relative to our estimated radial velocity uncertainty. Fig. 8 shows that restricting the sample to the 4 stars within the cluster radius from Sagar & Griffiths (1998) doesn't appreciably change the situation. One possibility is that the radial velocities for this cluster were more poorly determined than for the other clusters; there is, however, no evidence for this in the spectra so the spread in velocity must be real.

Examination of the CMD suggests that the initial colour selection was too wide. In light of the difficulty in isolating the cluster RGB, a wide net was cast in hopes that the cluster would reveal itself through a well-defined mean radial velocity distinct from the field. However, we unfortunately ended up with stars showing as wide a range in radial velocity as any stars in the entire field of the spectrograph. Considering the probable age of $\approx 1 \text{ Gyr}$ from Sagar & Griffiths (1998), and the richness of the Galactic field, this should probably have been anticipated and the algorithm for fibre assignments modified. Virtually all of the red giants within the cluster radius are RC stars, precisely those our algorithm tended to deweight. The rich background and sparse cluster upper RGB ensured that the bright stars we preferentially observed were those most likely to be nonmembers. Bearing this in mind, we deem it highly unlikely that we failed to observe *any* cluster members, and so we can try to weigh the various probabilities for membership.

Our initial, very liberal membership cut considered all stars within 1σ of the mean radial velocity of stars within $3'.6$ of the cluster center, $v_r = 5.4 \pm 34 \text{ km s}^{-1}$. This left us with six potential members, with an average velocity $v_r = -2.3 \pm 17.3 \text{ km s}^{-1}$. This can hardly be considered a restrictive cut, when the typical velocity dispersion of an open cluster is $\lesssim 1 \text{ km s}^{-1}$ (e.g., Mermilliod, Mayor & Udry 2008), comparable to our 1σ random velocity errors. All six of these stars are listed in Table 4, reflecting the uncertainty in identifying definite members.

We turned to photometric information for further guidance regarding the membership probabilities. The photometric catalogue of Sagar & Griffiths (1998) only covers the southern half of the cluster, and only includes two of our targets, although all 6 potential members lie within our adopted cluster radius and the radius given by Lyngå (1987). However, the limited optical photometry available does appear to rule out the membership of star 2MASS 19012993-0027231, which is far too bright and blue to be a cluster red giant (in the optical). This star also has a very different radial velocity from the remaining five potential members. That leaves two groups of stars that separate naturally into a group of three stars at positive radial velocity in a slightly brighter RGB, and a second group of two stars along a fainter track,

with negative radial velocity. In either case, we apparently have failed to measure any red clump stars, which if nothing else would have given much better leverage on the radial velocity. We have a marginal preference for the brighter subgroup, with $v_r = 13.0 \pm 4.2 \text{ km s}^{-1}$, for the following reasons: it includes the closest star to the cluster center; the RGB sequence is located in a favorable location relative to the red clump in the 2MASS CMD; and star 2MASS 19013595-00283878, which belongs to the fainter subgroup, was also flagged as a photometric outlier from the cluster RGB by Sagar & Griffiths (1998). With this in mind, we take the average metallicity, $[\text{Fe}/\text{H}] = -0.15 \pm 0.11$, of the brighter subgroup to be representative of the cluster.

Be 81 is our only inner galaxy cluster, lying just interior to the tangent point of the Sagittarius-Carina spiral arm ($\ell = 33.7$, $b = -2.5$). Accordingly, it is the most highly-reddened cluster in our sample, with $E(B - V) = 1.00$ (Dutra & Bica 2000). Sagar & Griffiths (1998) published the first CCD *BVI* photometry of Be 81 and derived the accepted distance of 3 kpc and an age of $t = 1 \text{ Gyr}$ for their estimate of approximately solar metallicity. Our derived metallicity, $[\text{Fe}/\text{H}] = -0.15 \pm 0.11$, is in agreement with this estimate. We can check for consistency with the distance and reddening measurements using the previously determined behaviour of the magnitude of the red clump, $\langle M_K \rangle$, as a function of cluster age and metallicity (Grocholski & Sarajedini 2002; Salaris & Girardi 2002). For our measured clump magnitude $K_{s,RC}$ from Table 2 and metallicity from Table 9 with the published age and reddening values, the tabulation of $\langle M_K \rangle$ in Salaris & Girardi (2002) yields a distance of 2.6 kpc, slightly shorter than the 3 kpc measure published by Sagar & Griffiths (1998). The 2MASS and optical CMDs are consistent with this distance, metallicity and reddening for the published age of 1 Gyr. If we had taken as members the fainter, redder red giants, they would be inconsistent with the position of the RGB from theoretical isochrones.

The radial velocity of Be 81 is ambiguous: the three preferred candidate members taken here have a mean velocity of $13.0 \pm 4.2 \text{ km s}^{-1}$, but the other two possible members are nearly identical to each other, with $v_r = -8.0 \pm 0.7 \text{ km s}^{-1}$ (however the brighter of the two was excluded from the cluster by Sagar & Griffiths (1998) on the basis of its $B - V$ colour). Neither velocity is remarkable compared to the nearby stellar field as observed here. Additionally, the disk kinematics near the galactic plane can be roughly assessed by comparison to the velocity profile of the neutral hydrogen, e.g., from Hartmann & Burton (1997). The HI in this part of the galaxy spans a very broad range of radial velocities, mostly receding from the Sun. Both possible radial velocities of Be 81 are well within the range of velocities for gas in the inner galaxy. Further, some deviation from the HI rotation curve is expected for old open clusters, which in general lag the thin disk rotation and show a significant number of eccentric galactic orbits (Scott, Friel & Janes 1995).

3.2 Berkeley 99

Like Be 81, the spectra for the Be 99 star sample were of good quality with only one star showing TiO bands. The radial velocity versus radial distance plot (Figure 8) shows a tight grouping of stars around $v_r \approx -60 \text{ km s}^{-1}$ which we

adopted to be cluster stars. The outer limit of the cluster was set at $r \approx 5'$ based on the 2MASS CMD, larger than the radius in Sagar & Griffiths (1998) (the most distant star in the final sample was $\approx 4'$ away). See Table 4 for information on the 9 stars in the final sample.

Be 99 and King 2 are the two clusters in our sample that are significantly outside the solar circle. Be 99 is both sparser and more distant than Be 81 (Sagar & Griffiths 1998), but also less reddened with $E(B-V) \approx 0.3-0.45$ (Dutra & Bica 2000; Schlegel, Finkbeiner & Davis 1998). Although Be 99 is higher off the Galactic plane than any of our other clusters ($b = +10$), its measured radial velocity is in excellent agreement with the HI rotation for its longitude ($\ell = 116$).

Be 99 has the lowest metallicity of any cluster in our sample, but it is not unusual for its galactocentric radius (Twarog, Ashman & Anthony-Twarog 1997; Friel et al. 2002). Its metallicity of $[\text{Fe}/\text{H}] = -0.58 \pm 0.10$ mandates a re-examination of its distance, age, and reddening. Comparison of theoretical isochrones to the 2MASS ($K_s, J - K_s$) CMD and to the data of Sagar & Griffiths (1998) reveals that the reddening $E(B-V)$ must be toward the high end of the published values: $E(B-V) \approx 0.43$. The lower metallicity and higher reddening combine to give consistency with the observed colour of the main sequence and RC. A downward revision of the age to ≈ 2.5 Gyr and retention of the accepted distance of 5 kpc (distance modulus $(m-M)_0 = 13.49$) reproduce the magnitude of the red clump in both K_s and I bands and is consistent with the main-sequence turnoff.

3.3 IC 1311

The star sample for IC 1311 contained only two low quality spectra with no stars showing contamination of TiO or CN bands. Inspection of the radial velocity versus radial distance plot (Figure 8) showed two groupings of stars, one around $v_r \approx -30 \text{ km s}^{-1}$ and the other at $v_r \approx -65 \text{ km s}^{-1}$. Attempts to identify trends in W' versus radial distance were of little help in determining which targets belonged to the cluster and which were field stars. We plotted both groupings on a 2MASS ($K_s, J - K_s$) colour-magnitude diagram (see Figure 11) in order to determine which locus each occupied. The grouping with $v_r \approx -65 \text{ km s}^{-1}$ traced the red giant branch more closely and was adopted as the cluster sample. The set of stars at this velocity is more centrally concentrated than the higher velocity set, and has a smaller range of velocities. Our final sample of 5 stars is listed in Table 4, and extends out to ≈ 4.5 radius, larger than the initial radius used to define the red clump magnitude but consistent with the visual appearance of the cluster.

The first CCD *UBVR* photometry of this relatively rich cluster was published by Delgado et al. (1994), who derived a distance of 6 kpc and an age of 1.6 Gyr for $[\text{Fe}/\text{H}] = 0$ and $E(B-V) = 0.28$ mag. The only other metallicity estimate of which we are aware is from the compilation of Tadross (2001), who estimated $[\text{Fe}/\text{H}] = -0.23$ (no uncertainty is given) based on the classical $(U-B)$ colour excess of the cluster. Our derived metallicity, $[\text{Fe}/\text{H}] = -0.30 \pm 0.16$, is not significantly different from either value but appears to confirm that IC 1311 has slightly subsolar metallicity. Adopting the age, distance, and reddening from Delgado et al. (1994) would produce a red clump

magnitude $K_{s,RC} = 12.48$, nearly half a magnitude brighter than observed. To adopt the reddening value advocated by Dutra & Bica (2000), $E(B-V) = 0.45$, would worsen the discrepancy, because consistency with the visible-light CMD would require a corresponding shift in distance modulus $\Delta(m-M)_0 \approx -0.5$ mag, producing an even brighter $K_{s,RC}$. Visual inspection of the Delgado et al. (1994) $(V, B-V)$ CMD combined with our observed $K_{s,RC}$ suggests that consistency can be achieved for a larger distance, $d \approx 6.6$ kpc, and a reddening in the range $0.3 < E(B-V) < 0.4$ mag. This requires a revision of the cluster age to $t \approx 1.1$ Gyr. An age near 1 Gyr is also consistent with the relatively high specific frequency of red clump stars in the cluster (Salaris & Girardi 2002). Note that the age listed in Dias et al. (2002) and in the online WEBDA database as of early 2008, $\log(t) = 8.625$, is obviously far too young to be consistent with the Delgado et al. (1994) or 2MASS CMDs. The revised distance puts IC 1311 clearly beyond the solar circle, but still within 10 kpc of the Galactic center for $R_0 = 8$ kpc. The measured heliocentric radial velocity of -63 km s^{-1} is in excellent agreement with the velocity of peak Galactic HI (thin disk) in this direction.

3.4 King 2

The stellar sample for King 2 had a larger quantity of poor-quality spectra than any of the other clusters in our sample. Fortunately all but two of the lower quality spectra stars fell outside of the adopted bounds of the cluster ($r \approx 5'$). The cluster radial velocity sequence was simple to pick out on the radial velocity versus radial distance plot (Figure 8) at around $v_r \approx -145 \text{ km s}^{-1}$. The final King 2 star sample consists of 7 stars (see Table 4).

King 2 is less studied than IC 1311 despite being of similar richness, distance, and reddening (e.g., Lyngå 1987; Dias et al. 2002). It certainly appears far less conspicuous on the sky, presumably because its greater age has truncated the main-sequence at much fainter magnitudes. The CMD study by Kałuzny (1989) resulted in a range of plausible ages and distances for different assumed reddenings and metallicities, while Aparicio et al. (1990) derived an age of 6 Gyr and a distance of 5.7 kpc for solar metallicity. Tadross (2001) derives the $(U-B)$ colour excess from the literature data and makes an estimate of $[\text{Fe}/\text{H}] = -0.32$ (no uncertainty given). Our CaT spectroscopy yields $[\text{Fe}/\text{H}] = -0.42 \pm 0.09$; for this metallicity, Kałuzny (1989) claims a most probable distance of 6.9 kpc and an age of ≈ 5 Gyr (see also Salaris et al. 2004). The metallicity is significantly subsolar, inconsistent with the finding by Aparicio et al. (1990). We find that a distance of 6.5 kpc and a slightly younger age, $t \approx 4$ Gyr, better fits the optical CMD and 2MASS $K_{s,RC}$ if the reddening $E(B-V) = 0.31$ from Dutra & Bica (2000) is adopted. The new distance puts it at $R_{GC} \approx 13$ kpc, where its metallicity falls close to the trend of the galactic abundance gradients derived in Friel et al. (2002). However, the observed radial velocity, $v_r = -144.2 \pm 5.9 \text{ km s}^{-1}$, differs by $\approx 100 \text{ km s}^{-1}$ from the rotation velocity of the gas disk at its longitude $\ell = 123^\circ$. This surprising deviation is discussed in detail in section 4 below.

3.5 NGC 7044

The star sample for NGC 7044 contained a large number of stars (6) showing the effects of TiO bands. These were the six brightest ($K_s < 8.02$) and reddest ($J - K_s > 1.39$) stars in the sample. Only three of these stars fell within the adopted cluster radius ($r \approx 6'$) while only one showed a similar radial velocity to the other adopted cluster stars ($v_r \approx -50 \text{ km s}^{-1}$). The adopted cluster stars showed a tight radial velocity grouping (Figure 8) with very little spread making the selection of members relatively straightforward. Table 4 lists the pertinent information for the ten stars in the NGC 7044 sample.

NGC 7044 is the most well-studied of the five clusters presented here, with three CCD photometric studies in the literature: (Kałużny 1989, Aparicio et al. 1993, and Sagar & Griffiths 1998). It has also been included in the overview of open cluster age measurements from cluster morphology in Salaris et al. (2004); the age measurements produced a range from 1.0–2.5 Gyr, and distances from 3–4 kpc. Because the metallicity $[\text{Fe}/\text{H}] = -0.16 \pm 0.09$ is consistent with the assumption of solar metallicity, no revision to the age is mandated by the new determination. However, consistency with $K_{s,RC}$ rules out a distance as high as 4 kpc. Adopting the reddening value $E(B - V) = 0.67$ from Dutra & Bica (2000), the 1 Gyr age of Salaris et al. (2004) yields a consistent $K_{s,RC}$ for $d = 3.2$ kpc, while the 1.6 Gyr age from Sagar & Griffiths (1998) requires $d \approx 3.6$ kpc. The latter pair of parameters provides greatest consistency with the CMD data from Aparicio et al. (1993) and Sagar & Griffiths (1998). Note that the 1.6 Gyr age is consistent with the conclusions of Delgado et al. (1994), who re-examined the data of Aparicio et al. (1993) in their study of IC 1311 and found that NGC 7044 is a few hundred Myr older than IC 1311. The new distance places NGC 7044 just beyond the solar circle. It has a slightly higher than typical metallicity, but lies within the scatter of the general galactic abundance gradient (Twarog, Ashman & Anthony-Twarog 1997; Friel et al. 2002). The radial velocity $v_r = -50.6 \pm 2.2 \text{ km s}^{-1}$ is in excellent agreement with the galactic rotation velocity of both HI and older disk stars (Hartmann & Burton 1997; Scott, Friel & Janes 1995; Carollo et al. 2007).

4 IS KING 2 ASSOCIATED WITH THE MONOCEROS STREAM?

The velocity distribution for the King 2 field is shown in Figure 8. The cluster clearly stands out, far from the general outer disk field along its sightline. We examined the predicted velocity distribution for stars at $\ell = 123^\circ$, $b = -5^\circ$ in the Besançon Galactic model of Robin et al. (2003); for heliocentric distances greater than 3 kpc, fewer than 1% of all disk stars in the model have both $v_r \leq -130 \text{ km s}^{-1}$ and $[\text{Fe}/\text{H}] \geq -0.5$, consistent with our easy identification of cluster members. The discrepant heliocentric radial velocity of King 2 compared to other disk populations leads us to look for possible explanations.

If King 2 is moving in pure circular motion, its observed radial velocity translates to an orbital speed of just 80 km s^{-1} , far too low to be a normal disk member. Conversely, disk membership and orbital speeds of 150–200 km

s^{-1} would imply large proper motions for the cluster as a large fraction of the motion would be perpendicular to the line of sight. Unfortunately, King 2 is the only cluster in our sample that does not have an estimated proper motion from Dias et al. (2006) or Kharchenko et al. (2003), so that three-dimensional velocity information is unavailable to help understand King 2's place in the Galaxy.

While many old open clusters follow eccentric galactic orbits (Scott, Friel & Janes 1995), King 2 is further out of synch with disk rotation than even Be 17, an anticentre cluster noted for its unusual radial velocity. Based on its relatively young age and location in the outer Galaxy, bulge membership would appear to be a poor explanation for the kinematics of King 2. However a disk origin within the solar circle may be plausible; if the entirety of King 2's motion is directed along its galactocentric radius vector, then it is moving radially *outward* at nearly 50 km s^{-1} . If on the other hand it is orbiting at typical thick disk speeds of $\approx 180 \text{ km s}^{-1}$, then it must be infalling at speeds in excess of 60 km s^{-1} . Whatever the true situation, it appears likely that King 2 is on a high-eccentricity, low angular momentum path around the Galaxy.

Assessing the degree to which King 2's motion is anomalous is hindered by the complexity of kinematics in this part of the galaxy. The Perseus spiral arm shows anomalous kinematics possibly related to its participation in a density wave, but lies 3–4 times closer to us than King 2 (Xu et al. 2006); On the far side of King 2, the high-velocity cloud Complex H (HVC130+01–161) overlaps in radial velocity with the cluster, but is probably several times more distant (Wakker 2001). Further complicating the picture, King 2 lies near on the sky to where several authors have found extensions of the structure known as the Monoceros stream (Newberg et al. 2002; Ibata et al. 2003; Yanny et al. 2003). Summaries of kinematic data pertaining to the Mon stream can be found in, e.g., Peñarrubia et al. (2005); Younger et al. (2008).

Could King 2 be a member of the Monoceros stream? Our favoured distance of ≈ 6.5 kpc places the cluster at a galactocentric distance of ≈ 13 kpc, consistent with but slightly interior to the Mon stream distance favoured by Ibata et al. (2003), and near the inner limit of detections reported from SDSS data in Newberg et al. (2002). Both Newberg et al. (2002) and Rocha-Pinto et al. (2003) detected Mon stream components among field stars at the longitude of King 2, but these earlier detections were at much higher positive and negative galactic latitude than King 2's relatively modest $b = -5^\circ$. Rocha-Pinto et al. (2004) measured radial velocities for stars over the longitude range from 103° – 163° , and their reported velocities correspond exactly to King 2's $v_r = -144 \text{ km s}^{-1}$; however, their measurements apparently pertain to stars averaging nearly 3 times farther away than King 2 (in the Triangulum-Andromeda structure). This, and the discrepant galactic latitudes, suggests that either the stream is extremely extended or the agreement is fortuitous. However, the distances found by Rocha-Pinto et al. (2004) are strongly metallicity dependent, and Rocha-Pinto et al. (2003) already noted the presence of a structure at closer distances. Further, the models of Peñarrubia et al. (2005) suggest that the majority of stars in the Monoceros stream should lie more nearby than the Tri-And structure, with similar radial velocities to the more distant stars.

If King 2 is indeed a member of the Monoceros stream, we might expect to see other stream members in the surrounding field. Rocha-Pinto et al. (2003) show that $\approx 10\%$ of the red giants in this general direction are distinct from the foreground of ordinary thick disk stars in their plots of relative distance vs. longitude. Of the 36 non-members we find in the King 2 field, two have radial velocities within the reported velocity dispersion of the stream measured by Rocha-Pinto et al. (2004), $\sigma_{v_r} = 20 \text{ km s}^{-1}$. Fig. 8 shows that these two stars have similar *reduced* CaT equivalent widths to the King 2 giants; however, since their distance isn't known, no accurate metallicity can be assigned to them. Their equivalent widths are consistent with being at the same distance and metallicity as King 2, but also with a distance 3 times larger and a metallicity 0.4 dex lower.

One interpretation of the Mon stream is as the tidally-disrupted remains of a satellite dwarf galaxy consumed in a minor merger with the Milky Way (e.g., Helmi et al. 2003; Martin et al. 2005). However, star clusters are uncommon in the known dwarf spheroidal (dSph) companions of the Milky Way: Fornax and Sagittarius host a few globular clusters each, but open clusters in dwarf spheroidals are unknown. Presumably this is not an absolute exclusion of open clusters in dSphs, but simply reflects the fact that star-formation rates have been low over longer timescales than the typical disruption time of a low-density cluster. Ownership of several globular clusters and open clusters has been attributed to the Monoceros stream and associated structures (e.g., Frinchaboy et al. 2004; Peñarrubia et al. 2005), although most of those have been towards the anticentre or third galactic quadrant and at larger distances. Detailed modelling, such as in Peñarrubia et al. (2005) has cast doubt on a number of these associations.

King 2's association with the Monoceros stream can remain only speculative in the absence of proper motion data, but it is an intriguing explanation for its anomalous kinematics. If the Monoceros stream does in fact claim King 2 as a member, then this could potentially shed light on the nature of the stream. If the Mon stream is really due to the dissolution of a 10^8 – $10^9 M_\odot$ dwarf galaxy in the plane of the Milky Way, then there may be multiple wraps of the tidal debris around the Galactic disk; the distance of King 2 would place it in the innermost of the rings, most recently stripped from its host. Its metallicity and galactic latitude might then help resolve some of the ambiguities in current models (e.g., Peñarrubia et al. 2005).

We also note that while King 2 has a higher metallicity than any dwarf galaxy except Sagittarius, it has a perfectly ordinary metallicity for an outer disk cluster (Twarog, Ashman & Anthony-Twarog 1997; Friel et al. 2002). Some controversy also persists as to the external, dwarf galaxy nature of both the Monoceros stream and the Canis Major dwarf (or overdensity) that is often taken to be the progenitor of the stream (e.g., Carraro, Moitinho, & Vázquez 2008). Younger et al. (2008) present detailed models of the high orbital eccentricity flyby of a large dwarf spheroidal, and show that the structure excited in the Milky Way disk strongly resembles a stream or ring similar to the Monoceros stream. King 2 may simply be an ordinary Milky Way old open cluster, participating in one of the ripples left in the wake of a satellite close en-

counter as described by Younger et al. (2008); this has the advantage of naturally accounting for King 2's metallicity.

5 DISCUSSION AND CONCLUSIONS

We have obtained near infrared spectra ($\lambda = 8416 - 8986 \text{ \AA}$) of 133 red giant stars from two Galactic globular clusters and ten Galactic open clusters and combined this sample with that of Cole et al. (2004). We used the calcium triplet lines to derive metallicities following the method pioneered by Armandroff & Da Costa (1991) and calibrated with Galactic globular clusters by Rutledge et al. (1997b). Our cluster sample spanned 2.2 dex in metallicity and 11 Gyr in age, comparable to the widest ranges in the literature to date (Carrera et al. 2007).

All prior studies of this technique that used both globular and open clusters (e.g., Cole et al. 2004; Carrera et al. 2007) have relied upon multiple literature sources for *VI* photometry. The use of numerous sources for photometry can lead to a non-uniform sample and could introduce non-linear effects in their calibration. Using 2MASS K_s photometry to calibrate our metallicity scale has the benefit of a uniform photometry sample for all stars down to $K_s \approx 14$. This is very important because it allows a unique opportunity to easily derive the metallicity for any Galactic cluster with only one new medium resolution spectra observation. If differential reddening plays a role, as it does in certain bulge globulars, use of K_s magnitudes will dramatically reduce its impact, perhaps allowing future studies to distinguish claims for internal abundance spreads from variable reddening.

Like others before us (e.g., Carretta et al. 2001; Cole et al. 2004; Carrera et al. 2007), our data show no signs of a non-linear relationship between CaT equivalent widths and metallicity. Therefore we can say that the slope of the best fit line in the ΣW versus $K_s - K_{s,HB}$ plane is independent of metallicity over the small range in magnitudes used in the RGB. We are able to use our calibration in estimating the $[\text{Fe}/\text{H}]$ values for five understudied Galactic open clusters (Be 81, Be 99, IC 1311, King 2, and NGC 7044). All of our metallicity estimates are statistically similar to estimates obtained by other methods, supporting the use of the calcium triplet plus 2MASS near-infrared magnitudes to derive $[\text{Fe}/\text{H}]$ for any cluster.

Calibrating the CaT - metallicity relation using 2MASS data has the added benefit in which any new observations in the K band can be calibrated to the 2MASS scale (Carpenter 2001). This allows our technique to be extended to extragalactic sources (i.e., the Magellanic clouds) and still retain uniformity. Future work can be done to use the tip of the RGB instead of the horizontal branch/red clump to define W' in terms of $(\mathfrak{M} - \mathfrak{M}_{TRGB})$. This would allow us to use the 2MASS photometry to estimate the metallicity of LMC/SMC clusters where 2MASS is not deep enough to reach the horizontal branch/red clump, obviating the need for new photometric data.

In order to derive the greatest benefit from this technique, we would like to use a uniform and consistent high-dispersion metallicity scale for both globular and open clusters. There are currently no studies for which a large sample of both families of clusters have had high-dispersion metallicities derived using atmospheric modelling. Because of this

our calibration is referred back to different reference scales in $[\text{Fe}/\text{H}]$ (Carretta & Gratton 1997; Friel et al. 2002). Our reported cluster reduced equivalent widths can be converted to any desired metallicity scale simply by rederiving the coefficients of the equation relating W' and $[\text{Fe}/\text{H}]$. Considering a very short list of alternative calibrator metallicities shows that the absolute calibration strongly changes at the high end, with clusters like Be 81 and NGC 7044 moving upward to solar metallicity if the latest high-dispersion abundances for clusters like NGC 6939 and NGC 7142 are chosen as the reference.

We report the first radial velocities and spectroscopic metallicities for five old open clusters chosen solely on the basis of their red giant content. In most cases the derived abundances are consistent with optical CMD morphology, the K_s -magnitude of the red clump, and published distance, age, and reddening estimates. The cluster Berkeley 81 was difficult to pick out from the field on the basis of radial velocity or CMD, re-emphasizing the limitations on such studies imposed by the generally sparse open cluster red giant numbers (Cannon 1970; Twarog, Ashman & Anthony-Twarog 1997). However, unambiguous cluster sequences were defined in the other four cases. Berkeley 99 was found to be the most metal-poor cluster in the understudied sample, with $[\text{Fe}/\text{H}] = -0.58 \pm 0.10$; the interplay between distance, reddening, and metallicity suggests that the age is slightly lower than reported in Sagar & Griffiths (1998). IC 1311 must be more distant than previously reported, at ≈ 6.6 kpc; it also must be significantly older than the 650 Myr reported in Carraro & Chiosi (1994). All clusters except King 2 were found to be unexceptional in their radial velocities (Scott, Friel & Janes 1995), with the caveat that the Be 81 velocity remains ambiguous because there was no clear way to distinguish between member and nonmember giants in the absence of a larger spectroscopic sample or more extensive optical photometry.

The cluster King 2 is strongly out of galactic rotation, lagging the disk by 60–100 km s⁻¹. Its heliocentric radial velocity $v_r = -144$ km s⁻¹ corresponds precisely to the velocities of stars in the Monoceros stream at its longitude of $\ell = 123^\circ$, although there may be discrepancies in distance and galactic latitude (Rocha-Pinto et al. 2004; Peñarrubia et al. 2005). Its metallicity $[\text{Fe}/\text{H}] = -0.42 \pm 0.09$ is high for a dwarf spheroidal origin, but very ordinary for old Milky Way open clusters. Apart from an extragalactic origin, King 2's velocity may be due to the ejection of an inner disk cluster into a high-eccentricity orbit due to interactions, e.g., with the Galactic bar, or to its participation in ripples induced in the wake of a satellite galaxy flyby (Younger et al. 2008). The possibilities cannot be disentangled in the absence of proper motion information.

ACKNOWLEDGMENTS

Travel support for AAC was provided by the Netherlands Research School for Astronomy (NOVA). We would like to thank our referee, Dr. Bruce Twarog, for his comments and suggestions that have greatly improved the manuscript. AAC would like to thank ING support astronomer Ian Skillen and night assistant Roberto Martinez for their able assistance during the observing run. Thanks to Professor

Linda Sparke for helpful information about the kinematics of the disk and to Professor Evan Skillman for helpful comments about the text. This publication makes use of data products from the Two Micron All Sky Survey, which is a joint project of the University of Massachusetts and IPAC/Caltech, funded by NASA and the NSF. This research has made use of the WEBDA database, operated at the Institute for Astronomy of the University of Vienna.

REFERENCES

- Alcaino, G., & Liller, W. 1986, *A&A*, 161, 61
- Anthony-Twarog, B. J., Twarog, B. A., & McClure, R. D. 1979, *ApJ*, 233, 188
- Aparicio, A., Bertelli, G., Chiosi, C., & Garcia-Pelayo, J.M. 1990, *Ap&SS*, 169, 37
- Aparicio, A., Alfaro, E.J., Delgado, A.J., Rodríguez-Ulloa, J.A., & Cabrera-Caño, J. 1993, *AJ*, 106, 1547
- Armandroff, T. E., & Da Costa, G. S. 1991, *AJ*, 101, 1329
- Battaglia, G., Irwin, M., Tolstoy, E., Hill, V., Helmi, A., Letarte, B., & Jablonka, P. 2008, *MNRAS*, 383, 183
- Bragaglia, A., et al. 2001, *AJ*, 121, 327
- Bragaglia, A., & Tosi, M. 2006, *AJ*, 131, 1544
- Burkhead, M. S., Burgess, R. D., & Haisch, B. M. 1972, *AJ*, 77, 661
- Cannon R.D. 1970, *MNRAS*, 150, 111
- Carollo, D. et al. 2007, *Nature*, 450, 1020
- Carpenter, J. M. 2001, *AJ*, 121, 2851
- Carraro, G., & Chiosi, C. 1994, *A&A*, 287, 761
- Carraro, G., Villanova, S., Demarque, P., McSwain, M. V., Piotto, G., & Bedin, L. R. 2006, *ApJ*, 643, 1151
- Carraro G., Moitinho A., & Vázquez R.A. 2008, *MNRAS*, 385, 1597
- Carrera, R., Gallart, C., Pancino, E., & Zinn, R. 2007, *AJ*, 134, 1298
- Carretta, E., & Gratton, R. G. 1997, *A&AS*, 121, 95
- Carretta, E., Cohen, J. G., Gratton, R. G., & Behr, B. B. 2001, *AJ*, 122, 1469
- Carretta E., Bragaglia A., & Gratton R. 2007, *A&A*, 473, 129
- Cole A.A., & Weinberg M.D. 2001, *BAAS*, 34, 573
- Cole, A. A., Smecker-Hane, T. A., & Gallagher, J. S., III 2000, *AJ*, 120, 1808
- Cole, A. A., Smecker-Hane, T. A., Tolstoy, E., Bosler, T. L., & Gallagher, J. S. 2004, *MNRAS*, 347, 367
- Crane J.D., Majewski S.R., Rocha-Pinto H.J., Frinchaboy P.M., Skrutskie M.F., & Law D.R. 2003, *ApJL*, 594, L119
- Delgado, A.J., Alfaro, E.J., Aparicio, A., & Cabrera-Caño, J. 1994, *AJ*, 108, 2193
- Dias, W.S., Alessi, B.S., Moitinho, A., & Lépine, J.R.D. 2002, *A&A*, 388, 168
- Dias, W.S., Assafin, M., Flório, V., Alessi, B.S., & LÍbero, V. 2006, *A&A*, 446, 949
- Dutra, C.M. & Bica, E. 2000, *A&A*, 359, 9
- Ferraro, F.R., Montegriffo, P., Origlia, L., & Fusi Pecci, F. 2000, *AJ*, 119, 1282
- Friel, E. D., & Janes, K. A. 1993, *A&A*, 267, 75
- Friel, E. D., Liu, T., & Janes, K. A. 1989, *PASP*, 101, 1105
- Friel, E. D., Janes, K. A., Tavaréz, M., Scott, J., Katsanis, R., Lotz, J., Hong, L., & Miller, N. 2002, *AJ*, 124, 2693
- Frinchaboy P.M., Majewski S.R., Crane J.D., Reid I.N.,

- Rocha-Pinto H.J., Phelps R.L., Patterson R.J., & Muñoz R.R. 2004, *ApJL*, 602, L21
- Gim, M., Vandenberg, D. A., Stetson, P. B., Hesser, J. E., & Zurek, D. R. 1998, *PASP*, 110, 1318
- Gratton, R. G., & Contarini, G. 1994, *A&A*, 283, 911
- Gratton, R. 2000, *Stellar Clusters and Associations: Convection, Rotation, and Dynamos*, 198, 225
- Gratton, R., Bragaglia, A., Carretta, E., & Tosi, M. 2006, *ApJ*, 642, 462
- Grocholski, A.J. & Sarajedini, A. 2002, *AJ*, 123, 1603
- Grocholski, A.J., Cole, A.A., Sarajedini, A., Geisler, D., & Smith, V.V. 2006, *AJ*, 132, 1630
- Gustafsson, B., Bell, R. A., Eriksson, K., & Nordlund, A. 1975, *A&A*, 42, 407
- Harris, W. E. 1975, *ApJS*, 29, 397
- Harris, W. E. 1996, *AJ*, 112, 1487
- Hartmann, D. & Burton W.B. 1997, “An Atlas of Galactic Neutral Hydrogen”, Cambridge Univ. Pr., Cambridge
- Helmi A, Navarro J.F., Meza A., Steinmetz M., & Eke V.R. 2003, *ApJL*, 592, L25
- Ibata R.A., Irwin M.J., Lewis G.F. & Ferguson A.M.N. 2003, *MNRAS*, 340, L21
- Jacobsen H.R., Friel E.D., & Pilachowski C.A. 2007, *AJ*, 134, 1216
- Jacobson, H. R., Friel, E. D., & Pilachowski, C. A. 2008, *AJ*, 135, 2341
- Jones, J.E., Alloin, D.M. & Jones, B.J.T. 1984, *ApJ*, 283, 457
- Jørgensen, U.G., Carlsson, M., & Johnson, H.R. 1992, *A&A*, 254, 258
- Kaluźny, J. 1989, *AcA*, 39, 13
- Kaluźny, J., & Richtler, T. 1989, *Acta Astronomica*, 39, 139
- Kharchenko, N.V., Pakulyak, L.K., & Piskunov, A.E. 2003, *ARep*, 47, 4
- Kraft, R. P., & Ivans, I. I. 2003, *PASP*, 115, 143
- Kurucz, R. L. 1992, *The Stellar Populations of Galaxies*, 149, 225
- Lee, S.-W. 1977, *ApJS*, 27, 381
- Lyngå G. 1987, *ESO Conf. Workshop Proc.*, 28, 379
- MacMinn, D., Phelps, R. L., Janes, K. A., & Friel, E. D. 1994, *AJ*, 107, 1806
- Martin N.F., Ibata R.A., Bellazzini F., Irwin M.J., & Lewis G.F. 2005, *MNRAS*, 362, 906
- Mermilliod J.-C., Mayor M., & Udry S. 2008, *A&A*, 485, 303
- Milone, A. A. E. 1994, *PASP*, 106, 1085
- Newberg, H.J. et al. 2002, *ApJ*, 569, 245
- Olszewski, E. W., Schommer, R. A., Suntzeff, N. B., & Harris, H. C. 1991, *AJ*, 101, 515
- Osterbrock, D.E., & Martel, A. 1991, *PASP*, 104, 76
- Peñarrubia, J., Martínez-Delgado, D., Rix, H.W., Gómez-Flechoso, M.A., Munn, J., Newberg, H. Bell, E.F., Yanny, B., Zucker, D., & Grebel, E.K. 2005, *ApJ*, 626, 128
- Pont, F., Zinn, R., Gallart, C., Hardy, E., & Winnick, R. 2004, *AJ*, 127, 840
- Robin A.C., Reylé C., Derrière S., & Picaud S., 2003, *A&A*, 409, 523
- Rocha-Pinto H.J., Majewski S.R., Skrutskie M.F., & Crane J.D. 2003, *ApJL*, 594, L115
- Rocha-Pinto H.J., Majewski S.R., Skrutskie M.F., Crane J.D., & Patterson R.J. 2004, *ApJ*, 615, 732
- Rutledge, G. A., Hesser, J. E., Stetson, P. B., Mateo, M., Simard, L., Bolte, M., Friel, E. D., & Copin, Y. 1997, *PASP*, 109, 883
- Rutledge, G. A., Hesser, J. E., & Stetson, P. B. 1997, *PASP*, 109, 907
- Sagar, R. & Griffiths, W.K. 1998, *MNRAS*, 299, 1
- Salaris, M., & Girardi, L. 2002, *MNRAS*, 337, 332
- Salaris, M., & Weiss, A. 2002, *A&A*, 388, 492
- Salaris, M., Weiss, A., & Percival, S. M. 2004, *A&A*, 414, 163
- Sanders, W. L. 1977, *ApJS*, 27, 89
- Schlegel D.J., Finkbeiner D.P. & Davis M. 1998, *ApJ*, 500, 525
- Scott J.E., Friel E.D., & Janes K.A. 1995, *AJ*, 109, 1706
- Skrutskie, M.F. 2006, *AJ*, 131, 1163
- Soderberg, A. M., Pilachowski, C. A., Barden, S. C., Willmarth, D., & Sneden, C. 1999, *PASP*, 111, 1233
- Stetson, P. B., & Harris, W. E. 1977, *AJ*, 82, 954
- Stetson, P. B. 1981, *AJ*, 86, 687
- Suntzeff, N. B., Mateo, M., Terndrup, D. M., Olszewski, E. W., Geisler, D., & Weller, W. 1993, *ApJ*, 418, 208
- Tadross, A.L. 2001, *New Astr.*, 6, 293
- Tautvaišienė, G., Edvardsson, B., Puzeras, E., & Ilyin, I. 2005, *A&A*, 431, 933
- Tonry, J., & Davis, M. 1979, *AJ*, 84, 1511
- Twarog, B.A., Ashman, K.M., & Anthony-Twarog, B.J. 1997, *AJ*, 114, 2556
- van Helshoecht V. & Groenewegen M.A.T. 2007, *A&A*, 463, 559
- Wakker B.P. 2001, *ApJS*, 136, 463
- Xu Y., Reid M.J., Zheng X.W., & Menten K.M., *Science*, 311, 54
- Yanny, B. et al. 2003, *ApJ*, 588, 824
- Yong D., Carney B.W., & Teixeira de Almeida M.L. 2005, *AJ*, 130, 597
- Yong, D., & Grundahl, F. 2008, *ApJL*, 672, L29
- Younger J.D., Besla G., Cox T.J., Hernquist L., Robertson B., & Willman B. 2008, *ApJL*, 676, L21
- Zinn, R., & West, M.J. 1984, *ApJS*, 55, 45

Table 1. Previously Measured Clusters

Cluster	α (J2000)	δ (J2000)	[Fe/H]	Age (Gyr)	$K_{s,RC}$	References
M15	21 ^h 29 ^m 58 ^s .3 ^a	+12°10′04″6 ^a	-2.12 ± 0.01	11.7	14.83 ± 0.35	1,2
M71	19 ^h 53 ^m 46 ^s .7 ^a	+18°46′45″7 ^a	-0.70 ± 0.03	10.2	11.83 ± 0.07	1,2
NGC 6791	19 ^h 20 ^m 50 ^s .7 ^a	+37°45′38″4 ^a	$+0.11 \pm 0.10$	10.2	11.48 ± 0.08	3,4
NGC 6819	19 ^h 41 ^m 14 ^s .5 ^a	+40°11′58″0 ^a	-0.11 ± 0.06	2.9	10.27 ± 0.11	3,4
NGC 6939	20 ^h 31 ^m 40 ^s .7 ^a	+60°39′34″5 ^a	-0.19 ± 0.09	2.1	9.89 ± 0.17	3,4
NGC 7142	21 ^h 45 ^m 03 ^s .8 ^a	+65°45′33″3 ^a	-0.10 ± 0.10	4.0	10.36 ± 0.30	3,4
NGC 7789	23 ^h 57 ^m 29 ^s .4 ^a	+56°43′38″4 ^a	-0.24 ± 0.09	1.8	10.05 ± 0.18	3,4
Cole et al. (2004) Clusters						
Berkeley 20	05 ^h 32 ^m 34 ^s	+00°10′	-0.61 ± 0.14	4.0	13.20 ± 0.15	3,4
Berkeley 39	07 ^h 46 ^m 45 ^s	−04°41′	-0.26 ± 0.09	7.0	11.54 ± 0.09	3,4
M67	08 ^h 51 ^m 25 ^s	+11°48′	-0.15 ± 0.05	4.3	7.95 ± 0.02	3,4
Melotte 66	07 ^h 26 ^m 28 ^s	−47°41′	-0.47 ± 0.09	5.3	11.74 ± 0.13	3,4
NGC 104	00 ^h 26 ^m 33 ^s	−71°51′	-0.70 ± 0.07	10.9	11.94 ± 0.12	1,4
NGC 1851	05 ^h 14 ^m 15 ^s	−40°04′	-0.98 ± 0.06	9.2	14.24 ± 0.18	2
NGC 1904	05 ^h 24 ^m 12 ^s	−24°31′	-1.37 ± 0.01	11.7	13.90 ± 0.30	1,2
NGC 2141	06 ^h 03 ^m 00 ^s	+10°30′	-0.33 ± 0.10	2.5	11.53 ± 0.10	3,4
NGC 2298	06 ^h 48 ^m 59 ^s	−36°00′	-1.74 ± 0.06	12.6	14.70 ± 0.20	1,2
NGC 4590	12 ^h 39 ^m 28 ^s	−26°45′	-1.99 ± 0.10	11.2	14.50 ± 0.10	1,2

^a Center of AF2/WYFFOS field.

References to metallicity and age values: (1) Carretta & Gratton (1997), (2) Salaris & Weiss (2002), (3) Friel et al. (2002), (4) Salaris et al. (2004).

Table 2. Clusters Without Previous Metallicity Determinations

Cluster	α (J2000) ^a	δ (J2000) ^a	ℓ (deg)	b (deg)	dist. (kpc)	Age (Gyr)	$K_{s,RC}$	Reference
Berkeley 81	19 ^h 01 ^m 40 ^s .2	−00°27′26″3	33.7	−2.5	3.0	1.0	11.27 ± 0.40	1
Berkeley 99	23 ^h 21 ^m 14 ^s .2	+71°46′50″7	116.0	+10.1	4.9	3.2	12.05 ± 0.14	1
IC 1311	20 ^h 10 ^m 49 ^s .4	+41°10′46″0	77.7	+4.2	5.3	1.1	12.96 ± 0.21	2
King 2	00 ^h 50 ^m 57 ^s .6	+58°11′20″8	122.9	−4.7	6.5	5.0	12.51 ± 0.10	3
NGC 7044	21 ^h 13 ^m 05 ^s .4	+42°29′47″0	85.9	−4.2	3.1	1.6	11.47 ± 0.19	1

^a Center of AF2/WYFFOS field.

References to age values: (1) Sagar & Griffiths (1998), (2) Delgado et al. (1994), (3) Kałuzny (1989).

Table 3. Defined Line and Continuum Bandpasses (Å)

Blue Continuum	Line	Red Continuum
8474-8489	8490-8506	8521-8531
8521-8531	8532-8552	8555-8595
8626-8650	8653-8671	8695-8725

Table 4. Sample of Cluster Giants and Derived Parameters^a

2MASS ID	K_s (mag)	σ_{K_s} (mag)	v_r (km s ⁻¹)	σ_{v_r} (km s ⁻¹)	$\Sigma W(\text{CaT})$ (Å)	σ_W (Å)	Notes
M15							
21295801+1214260	12.45	0.02	-108.79	2.04	3.39	0.35	
21295560+1212422	10.61	0.02	-112.75	1.66	3.83	0.17	
21294979+1212298	12.96	0.03	-108.12	2.25	2.94	0.37	
21294607+1211315	11.96	0.02	-108.56	1.76	3.86	0.32	
21294351+1210033	11.89	0.02	-104.09	1.60	3.45	0.28	
21294993+1208052	10.73	0.02	-99.23	1.38	4.08	0.24	
21300038+1207363	10.85	0.02	-100.52	0.94	3.80	0.19	RV template star
21300637+1206592	10.70	0.02	-108.89	0.03	3.91	0.26	RV template star
21300750+1208136	11.21	0.02	-111.78	1.16	4.01	0.20	
21301049+1210061	10.44	0.02	-98.90	1.13	4.82	0.21	
21301522+1211345	12.79	0.03	-111.59	1.79	3.11	0.44	
21300978+1212544	11.40	0.02	-99.89	1.17	4.14	0.27	
21300316+1213286	11.51	0.02	-109.68	0.01	3.63	0.24	RV template star
M71							
19534463+1851392	11.00	0.02	-23.44	1.22	6.65	0.19	
19533399+1849186	11.92	0.02	-22.98	1.46	6.49	0.25	
19533757+1847286	8.42	0.01	-29.65	1.32	8.23	0.18	
19533470+1846213	10.79	0.02	-26.82	1.09	6.86	0.31	
19532342+1845023	11.87	0.02	-20.34	1.73	6.53	0.22	
19533747+1844596	9.05	0.02	-27.65	1.05	7.80	0.16	
19533964+1841466	12.05	0.02	-26.69	1.21	6.74	0.30	
19534282+1846129	11.38	0.05	-24.03	1.37	7.16	0.42	
19535983+1844498	11.87	0.02	-24.38	1.11	6.10	0.21	
19535325+1846471	8.04	0.01	-23.96	1.05	8.60	0.17	
19535764+1847570	10.04	0.02	-27.75	1.26	6.89	0.18	
19535064+1849075	9.27	0.03	-27.15	0.77	7.55	0.17	
NGC 6791							
19204485+3746215	10.25	0.02	-44.52	0.66	9.31	0.26	
19203585+3746520	11.71	0.01	-49.93	0.98	8.59	0.35	
19204517+3744339	11.70	0.02	-51.31	0.73	9.15	0.36	
19205580+3742307	11.86	0.02	-48.25	1.08	9.22	0.37	
19210719+3744347	11.91	0.02	-46.29	0.89	8.23	0.29	
19205418+3746285	10.98	0.02	-44.59	0.69	9.00	0.32	
19205338+3748282	9.77	0.01	-50.72	0.77	9.49	0.22	
NGC 6819							
19410991+4015495	10.08	0.02	-0.12	0.03	8.04	0.24	RV template star
19410524+4014042	10.34	0.02	3.00	0.63	7.93	0.26	
19405020+4013109	10.35	0.02	2.17	1.24	8.03	0.23	
19405704+4010068	10.44	0.02	10.13	0.74	7.81	0.21	
19405797+4008174	10.17	0.02	-2.45	0.92	8.77	0.24	
19413031+4009005	7.90	0.02	3.19	0.74	9.33	0.26	
19412187+4011485	9.96	0.02	2.31	0.79	8.03	0.33	
19412147+4013573	10.25	0.02	-0.34	0.86	7.88	0.27	
19412222+4016442	10.31	0.02	-0.72	1.75	8.61	0.52	

^a Table 4 includes all of the stars which were used in the analysis. A version of Table 4 with all of the observed stars is available on the electronic edition of MNRAS.

Table 4 – *continued* Sample of Cluster Giants and Derived Parameters^a

2MASS ID	K_s (mag)	σ_{K_s} (mag)	v_r (km s ⁻¹)	σ_{v_r} (km s ⁻¹)	$\Sigma W(\text{CaT})$ (Å)	σ_W (Å)	Notes
NGC 6939							
20313338+6045507	9.80	0.02	-20.31	0.91	7.69	0.38	
20312540+6041164	10.03	0.02	-19.95	0.62	7.45	0.21	
20310597+6042139	9.56	0.02	-22.01	0.60	7.75	0.23	
20313200+6039271	9.81	0.02	-19.80	0.63	7.93	0.18	
20310189+6038116	9.72	0.02	-22.47	0.64	7.63	0.19	
20312693+6036595	8.55	0.02	-21.22	0.62	8.33	0.21	
20314054+6037084	7.97	0.02	-21.90	0.58	8.40	0.25	
20315345+6038573	10.23	0.02	-16.76	0.66	7.56	0.20	
20322403+6037398	9.80	0.02	-25.87	0.71	7.59	0.18	
20315931+6041075	9.95	0.02	-18.77	0.80	7.45	0.21	
20322172+6043113	8.33	0.02	-20.93	0.62	8.44	0.22	
20320790+6044167	9.83	0.02	-20.76	0.83	7.66	0.22	
20314339+6040386	9.84	0.02	-22.99	0.97	7.77	0.19	
NGC 7142							
21450182+6549286	9.82	0.03	-49.92	1.76	7.23	0.37	
21444497+6549144	8.67	0.02	-52.85	0.97	9.07	0.37	
21443881+6546382	10.49	0.02	-55.03	1.03	7.70	0.36	
21450252+6545401	7.55	0.01	-50.76	0.81	9.15	0.36	
21454049+6544561	8.77	0.02	-52.06	0.95	8.61	0.29	
21452095+6547402	9.15	0.02	-50.58	0.95	8.18	0.25	
NGC 7789							
23572445+5648304	7.55	0.02	-55.85	0.87	8.70	0.27	
23571692+5646200	8.67	0.01	-55.35	0.76	8.25	0.24	
23565473+5648163	9.98	0.02	-53.92	0.14	7.63	0.22	RV template star
23570324+5645580	5.89	0.01	-55.65	1.12	9.52	0.28	
23565546+5645091	8.84	0.02	-54.38	0.18	8.28	0.23	RV template star
23563303+5644332	10.05	0.02	-59.41	0.04	7.69	0.23	RV template star
23564587+5638407	9.73	0.01	-57.60	0.79	7.61	0.23	
23571400+5640586	8.85	0.01	-57.52	0.83	8.04	0.24	
23572501+5638363	9.97	0.02	-59.48	0.73	8.15	0.38	
23572872+5635228	10.32	0.02	-55.32	1.13	6.97	0.28	
23573184+5641221	8.04	0.01	-59.34	0.95	8.41	0.26	
23575156+5638566	5.81	0.02	-55.82	1.03	9.42	0.27	
23580133+5639219	9.42	0.02	-59.22	0.82	7.59	0.27	
23575204+5642256	6.73	0.02	-53.73	0.89	9.36	0.27	
23581624+5642054	10.29	0.02	-59.67	0.89	8.52	0.25	
23575501+5644323	8.90	0.02	-56.22	0.86	8.17	0.22	
23582319+5647371	8.15	0.01	-56.19	0.85	8.53	0.24	
23580015+5650125	8.34	0.02	-54.70	0.87	8.41	0.23	
23575149+5651040	8.08	0.01	-56.01	0.92	8.49	0.27	
23573079+5646443	10.13	0.02	-55.65	0.75	7.61	0.22	
Be 81							
<i>Brighter subgroup (see §3.1)</i>							
19013063-0024456	8.58	0.02	15.84	0.98	9.61	0.34	
19015206-0026466	10.61	0.02	14.24	1.02	7.81	0.26	
19013928-0026285	10.19	0.03	7.82	1.12	8.27	0.62	
<i>Fainter subgroup (see §3.1)</i>							
19013687-0024097	10.52	0.02	-8.37	1.00	7.82	0.37	
19013595-0028378	9.65	0.02	-7.40	1.26	8.99	0.32	
<i>Photometric outlier (see §3.1)</i>							
19012993-0027231	9.09	0.02	-29.39	0.90	8.22	0.22	

^aTable 4 includes all of the stars which were used in the analysis.
A version of Table 4 with all of the observed stars is available on
the electronic edition of MNRAS.

Table 4 – *continued* Sample of Cluster Giants and Derived Parameters^a

2MASS ID	K_s (mag)	σ_{K_s} (mag)	v_r (km s ⁻¹)	σ_{v_r} (km s ⁻¹)	$\Sigma W(\text{CaT})$ (Å)	σ_W (Å)	Notes
Be 99							
23204241+7148166	12.06	0.03	-64.27	1.72	6.62	0.30	
23204335+7146540	11.16	0.02	-66.85	1.24	7.08	0.20	
23210175+7145598	8.61	0.02	-61.61	0.88	8.50	0.20	
23205404+7143296	11.35	0.02	-70.97	0.95	7.79	0.28	
23213138+7143175	12.34	0.02	-51.50	1.62	6.58	0.28	
23213173+7146053	11.48	0.02	-64.40	1.93	6.55	0.23	
23215512+7146502	11.33	0.02	-47.01	1.49	6.85	0.25	
23213813+7147350	11.20	0.03	-62.54	1.29	5.41	0.84	
23212213+7148034	9.11	0.02	-61.12	0.75	8.47	0.23	
IC 1311							
20104659+4112343	8.46	0.01	-61.45	1.06	10.70	0.32	
20103943+4114014	13.16	0.04	-61.71	1.74	8.11	0.56	
20104386+4110029	10.78	0.01	-64.19	1.23	7.77	0.28	
20103623+4107222	11.21	0.01	-64.42	1.24	8.19	0.29	
20105457+4112248	13.06	0.03	-65.14	2.08	6.11	0.61	
King 2							
00504698+5815418	11.29	0.02	-144.48	1.13	7.23	0.47	
00503676+5808417	11.98	0.02	-151.15	2.18	6.65	0.57	
00505902+5808216	12.57	0.02	-147.13	2.68	7.10	0.69	
00511367+5807532	11.71	0.02	-132.75	2.02	7.53	0.61	
00510072+5810562	10.04	0.02	-144.70	3.40	8.58	0.28	
00511598+5813527	11.51	0.02	-147.99	4.47	7.48	0.69	
00505610+5812053	12.38	0.02	-147.25	2.35	7.61	0.64	
NGC 7044							
21130270+4231244	10.74	0.02	-49.19	0.98	8.55	0.27	
21130119+4229295	11.39	0.02	-55.10	1.53	6.80	0.47	
21124797+4231110	11.70	0.02	-50.42	1.60	8.58	0.55	
21124114+4229229	10.56	0.01	-52.53	1.15	8.67	0.46	
21123464+4228075	10.49	0.02	-49.32	0.93	8.02	0.29	
21130646+4228414	10.00	0.02	-49.54	0.93	8.73	0.35	
21133247+4230482	10.86	0.02	-53.91	1.09	8.13	0.34	
21131398+4229449	10.08	0.01	-49.57	1.15	8.10	0.31	
21131533+4231270	11.40	0.02	-50.20	1.04	8.20	0.30	
21131452+4235234	11.37	0.02	-49.24	1.10	7.49	0.34	

^aTable 4 includes all of the stars which were used in the analysis. A version of Table 4 with all of the observed stars is available on the electronic edition of MNRAS.

Table 5. Sample of Cluster Giants from Cole et al. (2004) and Derived Parameters^a

ID ^b	K_s (mag)	σ_{K_s} (mag)	v_r (km s ⁻¹)	σ_{v_r} (km s ⁻¹)	$\Sigma W(\text{CaT})$ (Å)	σ_W (Å)
Be 20: MacMinn et al. (1994)						
022	14.31	0.08	74.6	7.5	6.19	0.03
008	11.85	0.03	79.2	7.5	7.41	0.02
005	11.35	0.02	73.9	7.5	7.56	0.02
012	13.25	0.04	83.8	7.5	6.61	0.02
Be 39: Kalużny & Richtler (1989)						
KR009	11.43	0.02	56.7	7.5	7.14	0.03
KR002	9.05	0.02	56.5	7.5	8.39	0.03
KR012	11.56	0.02	55.9	7.4	7.37	0.03
KR005	10.55	0.03	56.5	7.5	7.68	0.03
KR013	11.56	0.02	58.2	7.5	6.87	0.03
KR018	11.69	0.03	57.9	7.5	6.88	0.03
KR017	11.82	0.02	54.0	7.6	6.72	0.03
KR016	11.62	0.02	61.4	7.5	7.28	0.03
KR003	9.79	0.02	61.0	7.4	8.26	0.03
KR028	12.61	0.03	58.9	7.5	6.6	0.03
M67: Sanders (1977)						
F104	8.61	0.02	33.5	-	7.13	0.16
F164	7.96	0.02	33.3	-	7.4	0.15
F105	7.39	0.02	34.3	-	8	0.16
F141	7.94	0.02	33.6	-	7.73	0.14
F170	6.49	0.02	34.3	-	8.28	0.19
F135	8.95	0.02	34.3	-	7.1	0.13
F108	6.49	0.02	34.7	-	8.36	0.17
Mel 66: Anthony-Twarog et al. (1979)						
1205	11.82	0.03	18.3	7.5	6.86	0.11
2261	10.56	0.02	41.2	7.5	7.46	0.16
2244	11.83	0.03	16.4	7.6	6.97	0.09
2233	12.81	0.03	14.4	7.4	6.51	0.09
2226	11.20	0.02	18.9	7.5	7.11	0.19
2133	9.54	0.02	10.9	7.5	7.91	0.12
2107	11.77	0.02	14.9	7.5	6.57	0.11
3260	11.56	0.04	16.2	7.4	6.9	0.12
3133	10.96	0.02	17.2	7.6	6.98	0.12
3235	11.82	0.02	18.3	7.7	6.89	0.10
4151	8.84	0.02	12.7	7.6	8.23	0.13
4265	10.98	0.02	7.4	7.5	6.97	0.12
3229	10.93	0.02	7.7	7.5	7.08	0.31

^aTable 5 includes all of the stars which were used in the analysis.^bReferences are for star IDs.

Table 5 – *continued* Sample of Cluster Giants from Cole et al. (2004) and Derived Parameters^a

ID ^b	K_s (mag)	σ_{K_s} (mag)	v_r (km s ⁻¹)	σ_{v_r} (km s ⁻¹)	$\Sigma W(\text{CaT})$ (Å)	σ_W (Å)
NGC 104: Lee (1977)						
L5309	8.64	0.02	-21.8	7.6	7.98	0.10
L5312	8.54	0.02	-12.3	7.5	7.91	0.10
L5418	12.98	0.03	-20.6	7.9	5.77	0.16
L5422	9.09	0.02	-23.1	7.6	7.38	0.10
L5419	11.81	0.02	-22.2	7.8	6.13	0.12
L5527	10.85	0.02	-25.5	7.6	6.79	0.09
L5530	9.87	0.02	-18.6	7.6	6.92	0.08
NGC 1851: Stetson (1981)						
003	10.30	0.02	324.5	7.4	7.52	0.02
065	13.56	0.06	322.1	7.5	5.67	0.03
095	10.09	0.02	334.1	7.4	6.94	0.02
126	11.39	0.02	321.5	7.5	6.95	0.02
123	14.06	0.06	329.7	7.4	4.99	0.03
112	10.38	0.02	327.3	7.4	6.85	0.03
109	12.12	0.02	334.3	7.4	5.96	0.03
275	12.39	0.03	333.8	7.6	6.79	0.03
160	13.17	0.04	326.4	7.7	5.85	0.03
209	11.24	0.03	333.4	7.6	7.05	0.02
107	11.52	0.02	330.7	7.5	6.78	0.03
231	13.56	0.05	332.8	7.8	5.89	0.03
175	13.82	0.05	332.3	7.9	6.07	0.04
195	13.34	0.03	327.6	7.5	5.75	0.03
179	14.23	0.07	320.4	7.8	5.66	0.03
NGC 1904: Stetson & Harris (1977)						
6	12.85	0.03	203.2	7.4	4.91	0.03
11	13.48	0.05	213.5	7.5	4.85	0.03
45	13.21	0.04	206.8	7.8	4.95	0.05
15	9.99	0.02	204.8	7.5	6.67	0.02
241	10.72	0.02	228.5	7.5	5.8	0.02
237	11.32	0.02	220.8	7.5	5.77	0.02
89	12.13	0.02	206.5	7.8	5.51	0.02
91	14.18	0.07	207.6	7.8	4.76	0.05
224	13.88	0.05	220.4	7.9	4.63	0.05
111	13.21	0.05	206.9	7.6	5.18	0.03
115	13.72	0.06	211.0	7.7	4.65	0.05
138	14.00	0.07	206.3	7.8	4.36	0.04
153	10.26	0.02	206.1	7.4	6.47	0.02
209	12.43	0.03	210.8	7.5	5.63	0.02
160	9.61	0.02	200.3	7.5	6.42	0.02
161	13.68	0.05	216.5	7.8	4.05	0.05
176	12.52	0.03	215.9	7.6	4.74	0.02

^aTable 5 includes all of the stars which were used in the analysis.^bReferences are for star IDs.

Table 5 – *continued* Sample of Cluster Giants from Cole et al. (2004) and Derived Parameters^a

ID ^b	K_s (mag)	σ_{K_s} (mag)	v_r (km s ⁻¹)	σ_{v_r} (km s ⁻¹)	$\Sigma W(\text{CaT})$ (Å)	σ_W (Å)
NGC 2141: Burkhead et al. (1972)						
5-09	11.31	0.02	33.0	7.5	7.69	0.03
5-13	10.33	0.02	32.0	7.5	7.92	0.03
4-08	11.58	0.03	23.2	7.6	7.76	0.03
4-09	8.98	0.02	28.7	7.6	8.78	0.03
4-13	11.77	0.03	32.1	7.4	6.79	0.03
4-14	12.30	0.03	28.8	7.4	7.38	0.03
3-2-52	10.85	0.02	33.2	7.5	7.67	0.03
3-2-40	8.86	0.02	28.9	7.4	8.8	0.03
3-2-34	11.57	0.02	27.6	7.5	7.26	0.03
3-2-18	8.34	0.02	26.0	7.5	9.35	0.03
1-4-05	10.61	0.02	50.0	7.5	7.58	0.03
1-3-21	10.33	0.02	31.8	7.5	8.04	0.03
4-25	10.32	0.02	31.3	7.5	8.11	0.03
4-24	11.63	0.03	31.4	7.5	7.64	0.02
NGC 2298: Alcaïno & Liller (1986)						
AL12	11.06	0.03	146.6	7.5	4.84	0.02
AL15	11.77	0.02	151.2	7.6	4.31	0.02
AL6	10.55	0.03	156.5	7.6	4.97	0.02
AL22	12.49	0.03	162.0	7.4	4.06	0.02
AL25	13.05	0.04	153.2	7.5	4.15	0.02
NGC 4590: Harris (1975)						
I-258	11.86	0.02	-90.2	7.7	3.14	0.02
I-256	9.81	0.02	-90.9	7.6	5.2	0.02
I-260	9.51	0.02	-91.9	7.5	4.85	0.02
I-2	12.83	0.05	-96.0	7.6	2.98	0.02
I-239	11.71	0.03	-86.0	7.6	3.63	0.02
I-49	12.68	0.03	-93.6	7.8	3.04	0.02
I-74	12.20	0.02	-103.7	7.7	3.21	0.02
I-119	10.92	0.02	-89.1	7.6	3.78	0.02
II-47	12.76	0.02	-85.8	7.8	3.19	0.02

^aTable 5 includes all of the stars which were used in the analysis.^bReferences are for star IDs.

Table 6. Comparison to Previous Measurements

Cluster	W' (Å)	[Fe/H]	[Fe/H] $_{ref}^a$	v_r (km s $^{-1}$)	$v_{r,ref}$ (km s $^{-1}$)	Reference b
M15	2.17 ± 0.07	-2.04 ± 0.07	-2.12 ± 0.01	-109.5 ± 0.0	-107.0 ± 0.2	1
M71	6.48 ± 0.08	-0.61 ± 0.08	-0.70 ± 0.03	-25.8 ± 0.3	-22.8 ± 0.2	1
NGC 6791	8.84 ± 0.13	0.18 ± 0.08	0.11 ± 0.10	-47.6 ± 0.3	-47.1 ± 0.8	2
NGC 6819	8.13 ± 0.11	-0.06 ± 0.08	-0.11 ± 0.06	-0.1 ± 0.0	-7.0 ± 13.0	3
NGC 6939	7.63 ± 0.03	-0.22 ± 0.07	-0.19 ± 0.09	-21.0 ± 0.2	-19.0 ± 0.2	4
NGC 7142	7.71 ± 0.17	-0.20 ± 0.09	-0.10 ± 0.10	-52.0 ± 0.4	-44.0 ± 12.0	3
NGC 7789	7.61 ± 0.07	-0.23 ± 0.07	-0.24 ± 0.09	-58.6 ± 0.0	-57.0 ± 7.0	3

^a References to [Fe/H] $_{ref}$ values are given in Table 1.

^b References to $v_{r,ref}$ are: (1) Harris (1996), (2) Carraro et al. (2006), (3) Friel et al. (1989), and (4) Milone (1994).

Table 7. Comparison to Previous Measurements

Cole et al. (2004) Cluster	W' (Å)	[Fe/H]	[Fe/H] $_{ref}^a$	[Fe/H] $_{C04}^b$
Berkeley 20	6.70 ± 0.03	-0.53 ± 0.07	-0.61 ± 0.14	-0.47 ± 0.07
Berkeley 39	7.14 ± 0.06	-0.39 ± 0.07	-0.26 ± 0.09	-0.32 ± 0.09
M67	7.59 ± 0.05	-0.24 ± 0.07	-0.15 ± 0.05	-0.19 ± 0.05
Melotte 66	6.82 ± 0.17	-0.50 ± 0.09	-0.47 ± 0.09	-0.48 ± 0.06
NGC 104	6.17 ± 0.06	-0.71 ± 0.07	-0.70 ± 0.07	-0.66 ± 0.09
NGC 1851	5.41 ± 0.09	-0.96 ± 0.08	-0.98 ± 0.06	-0.96 ± 0.12
NGC 1904	4.55 ± 0.07	-1.25 ± 0.07	-1.37 ± 0.01	-1.37 ± 0.11
NGC 2141	7.48 ± 0.07	-0.27 ± 0.07	-0.33 ± 0.10	-0.26 ± 0.10
NGC 2298	3.07 ± 0.08	-1.74 ± 0.07	-1.74 ± 0.06	-1.69 ± 0.07
NGC 4590	2.27 ± 0.10	-2.00 ± 0.08	-1.99 ± 0.10	-2.07 ± 0.09

^a References to [Fe/H] $_{ref}$ values are given in Table 1.

^b Metallicity values defined by equation 5 of Cole et al. (2004).

Table 8. Comparison to Previous Measurements

Cluster	$[\text{Fe}/\text{H}]_{ref}$	$[\text{Fe}/\text{H}]_{line}$	$[\text{Fe}/\text{H}]_{quad}$	Reference ^a
Berkeley 20	-0.44 ± 0.13	-0.43 ± 0.13	-0.54 ± 0.10	8
M67	-0.03 ± 0.03	-0.08 ± 0.13	-0.10 ± 0.10	7
Melotte 66	-0.38 ± 0.15	-0.38 ± 0.15	-0.48 ± 0.13	5
NGC 104	-0.67 ± 0.03	-0.63 ± 0.13	-0.77 ± 0.10	2
NGC 1851	-1.27 ± 0.03	-0.93 ± 0.13	-1.09 ± 0.11	9
NGC 1904	-1.37 ± 0.05	-1.26 ± 0.13	-1.41 ± 0.10	3
NGC 2141	-0.18 ± 0.15	-0.12 ± 0.13	-0.16 ± 0.11	8
NGC 2298	-1.74 ± 0.06	-1.84 ± 0.13	-1.88 ± 0.10	3
NGC 4590	-2.00 ± 0.03	-2.15 ± 0.14	-2.09 ± 0.10	3
M15	-2.12 ± 0.01	-2.19 ± 0.13	-2.11 ± 0.10	3
M71	-0.70 ± 0.03	-0.51 ± 0.13	-0.63 ± 0.11	3
NGC 6791	0.47 ± 0.04	0.41 ± 0.14	0.56 ± 0.12	4
NGC 6819	0.09 ± 0.03	0.13 ± 0.14	0.18 ± 0.12	1
NGC 6939	0.06 ± 0.06	-0.06 ± 0.13	-0.08 ± 0.10	6
NGC 7142	0.14 ± 0.06	-0.03 ± 0.15	-0.04 ± 0.13	6
NGC 7789	-0.04 ± 0.05	-0.07 ± 0.13	-0.09 ± 0.11	7

Predicted metallicities when high-dispersion metallicity estimates from multiple sources are used in the calibration.

^a References to $[\text{Fe}/\text{H}]_{ref}$ values are: (1) Bragaglia et al. (2001), (2) Carretta, Bragaglia & Gratton (2007), (3) Carretta & Gratton (1997), (4) Gratton et al. (2006), (5) Gratton & Contarini (1994), (6) Jacobson et al. (2008), (7) Tautvaišienė et al. (2005), (8) Yong, Carney & Teixeira (2005), (9) Yong & Grundahl (2008).

Table 9. Cluster Velocities and Metallicities

Cluster	W' (Å)	$[\text{Fe}/\text{H}]$	v_r (km s ⁻¹)
Be 81	7.85 ± 0.25	-0.15 ± 0.11	13.00 ± 4.24
Be 99	6.57 ± 0.23	-0.58 ± 0.10	-62.28 ± 7.46
IC 1311	7.40 ± 0.44	-0.30 ± 0.16	-63.15 ± 1.79
King 2	7.04 ± 0.15	-0.42 ± 0.09	-144.25 ± 5.92
NGC 7044	7.83 ± 0.17	-0.16 ± 0.09	-50.56 ± 2.18

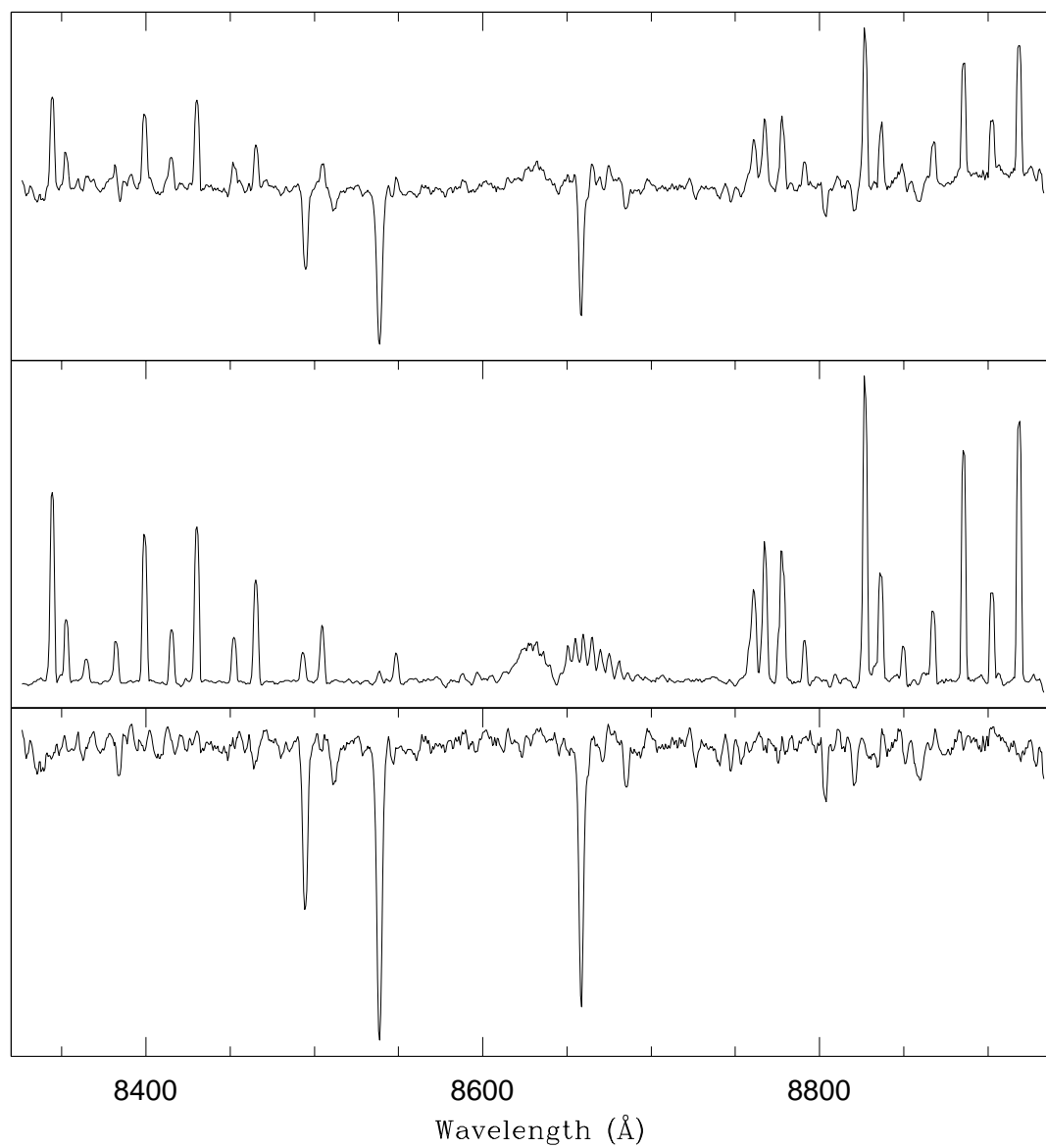


Figure 1. The raw spectrum, offset sky, and reduced spectrum (continuum normalized) for a typical target star (M15 #21300038+1207363).

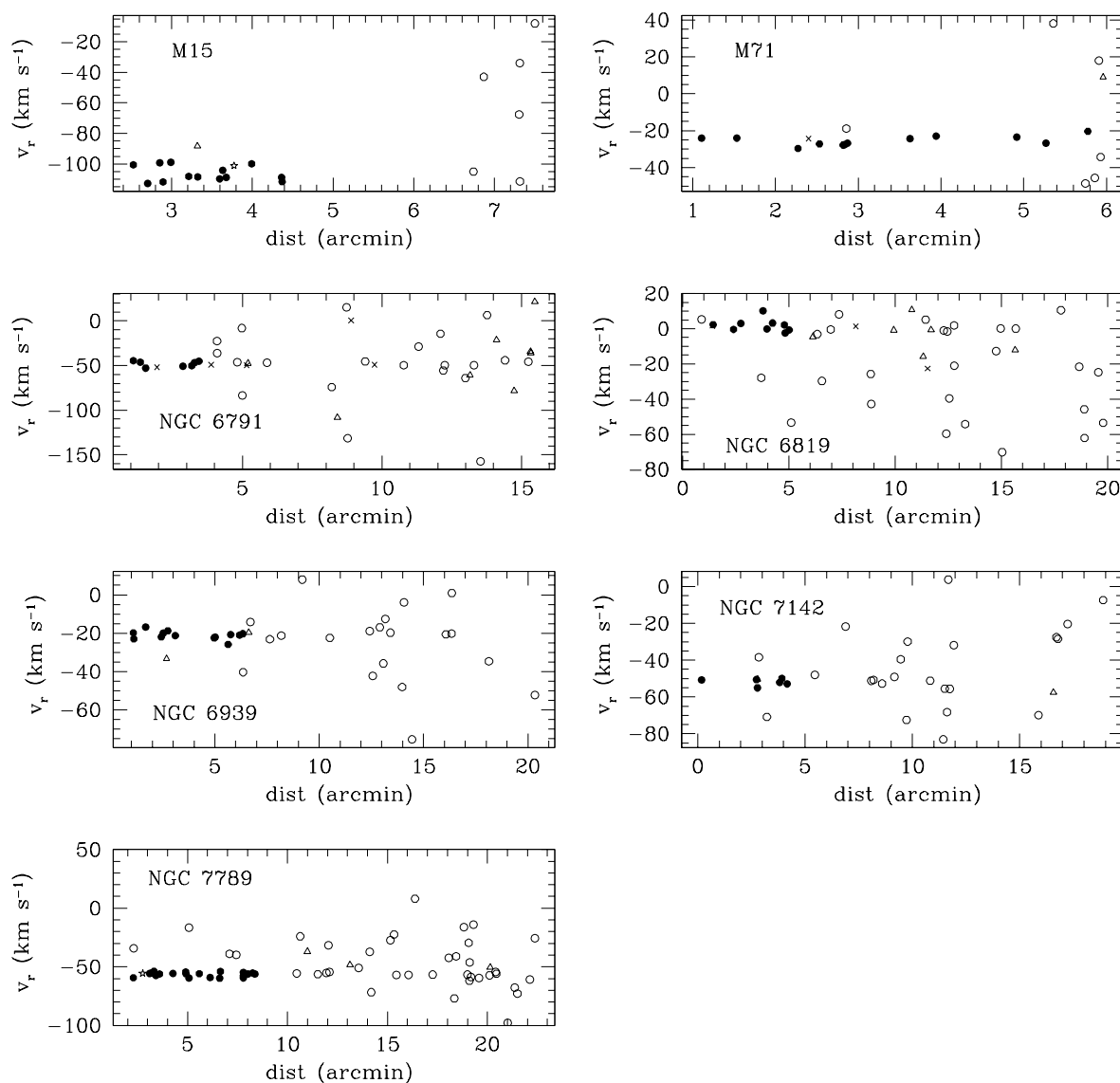


Figure 2. Filled black circles are the accepted cluster stars based upon radial velocity and positional determinations. Open symbols are stars rejected from further analysis based upon radial velocities/falling beyond the visual cluster bounds (circles), TiO bands (crosses), CN bands (stars), and/or low quality spectra (triangles).

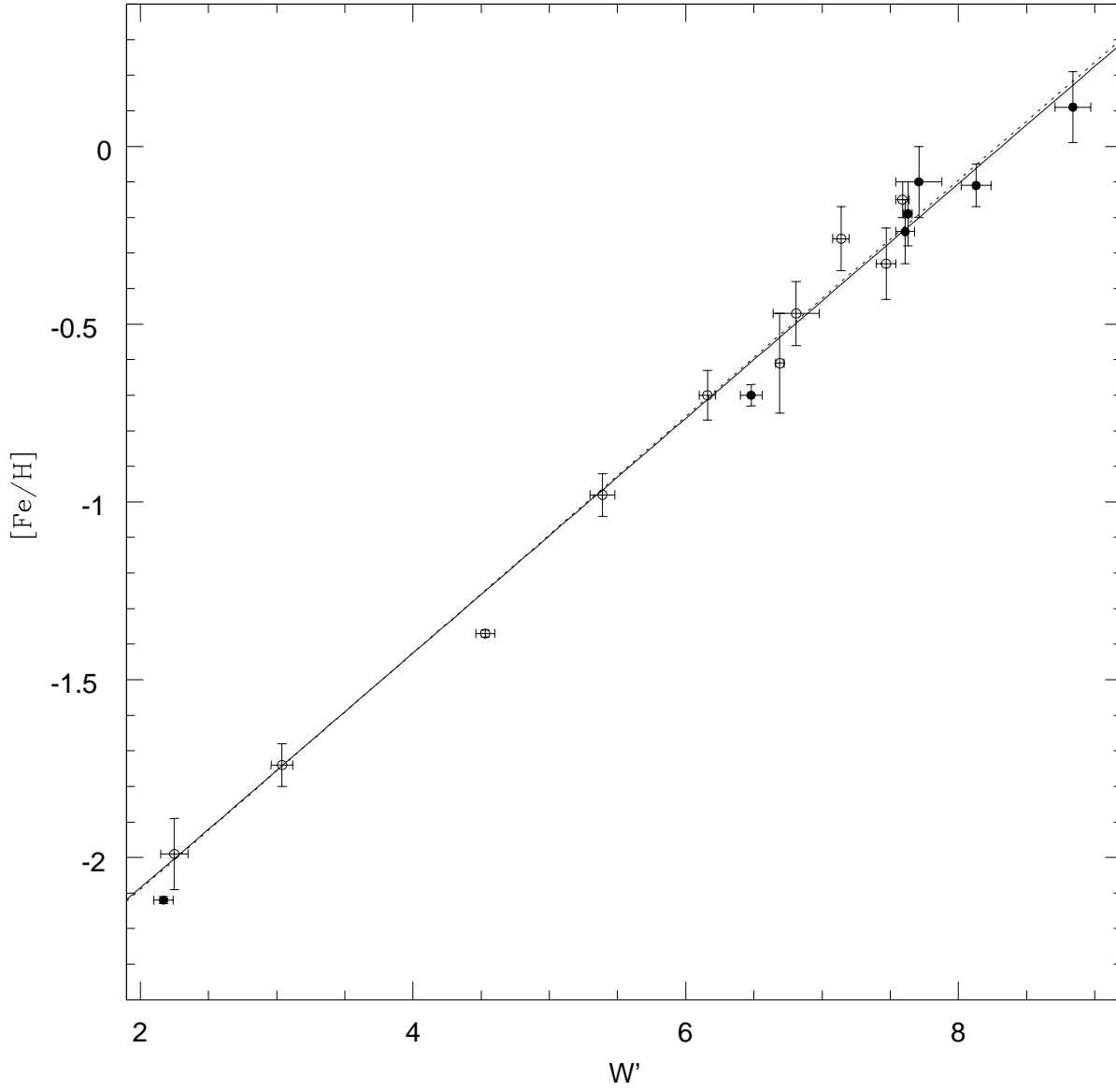


Figure 3. Filled circles and the best fit solid line are for our cluster sample. Open circles and the best fit dashed line represent the clusters of the Cole et al. (2004) sample.

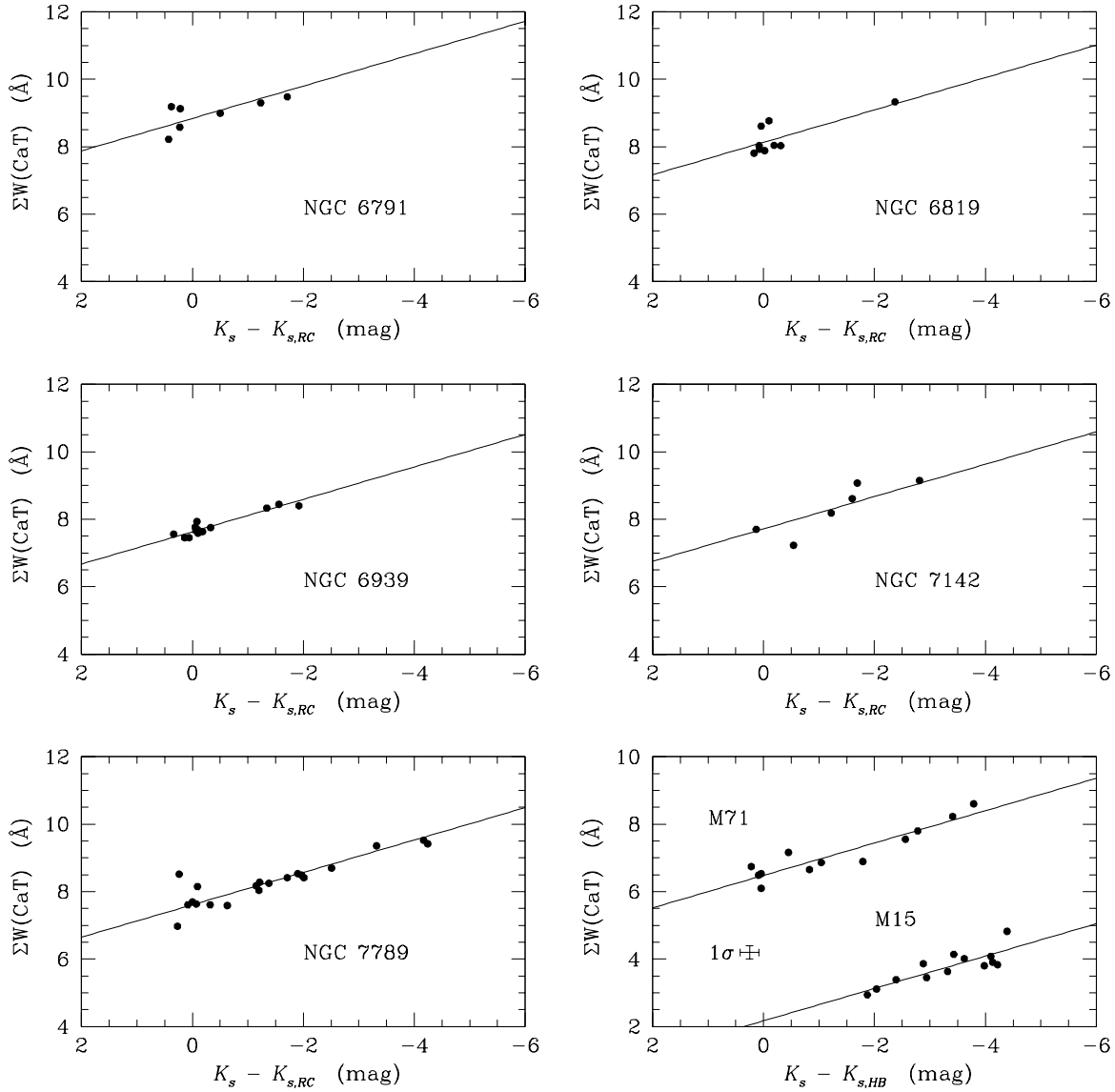


Figure 4. The best fit line using $\beta_{K_s} = 0.48$ as the slope for each of our calibration clusters. The typical 1σ errors for the points are in the bottom right panel.

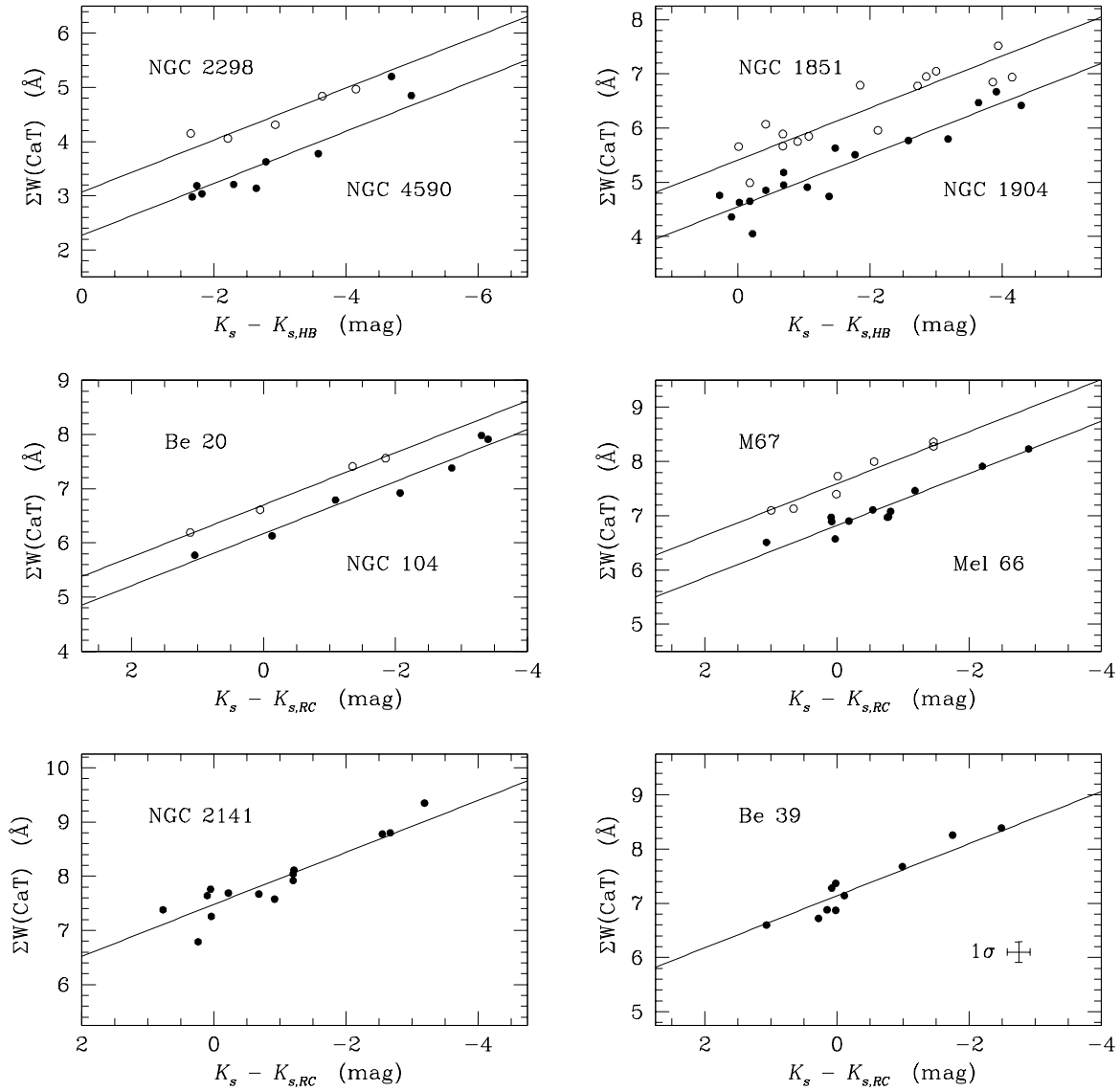


Figure 5. The best fit line using $\beta_{K_s} = 0.48$ as the slope for each of the Cole et al. (2004) calibration clusters. The typical 1σ errors for the points are in the bottom right panel.

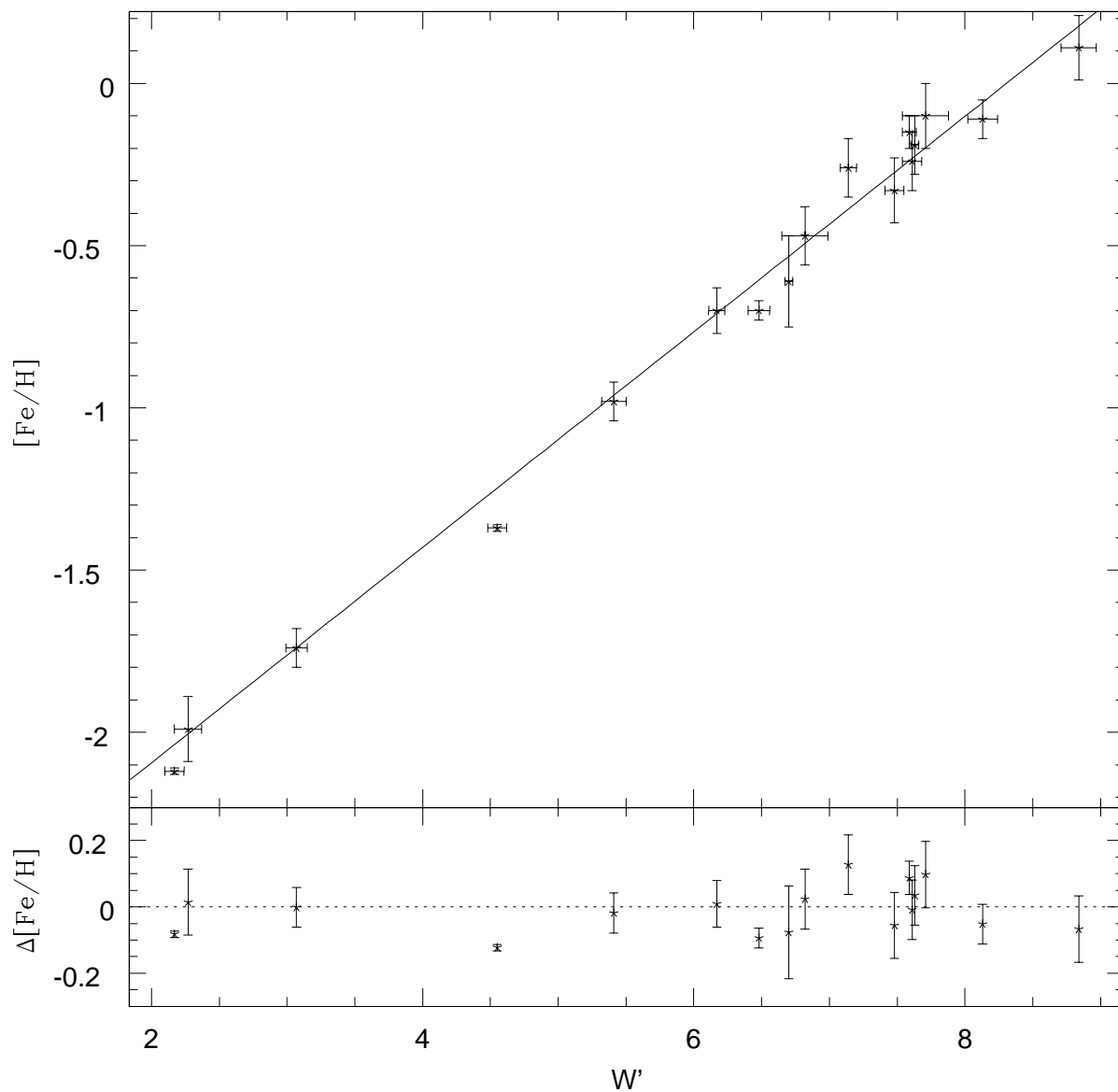


Figure 6. Top Panel: Calibration cluster metallicities from Table 1 plotted versus their W' values. The weighted (by metallicity) best fit line is also shown. Bottom panel: Residuals to the best fit line with the 1σ reference metallicity errors shown.

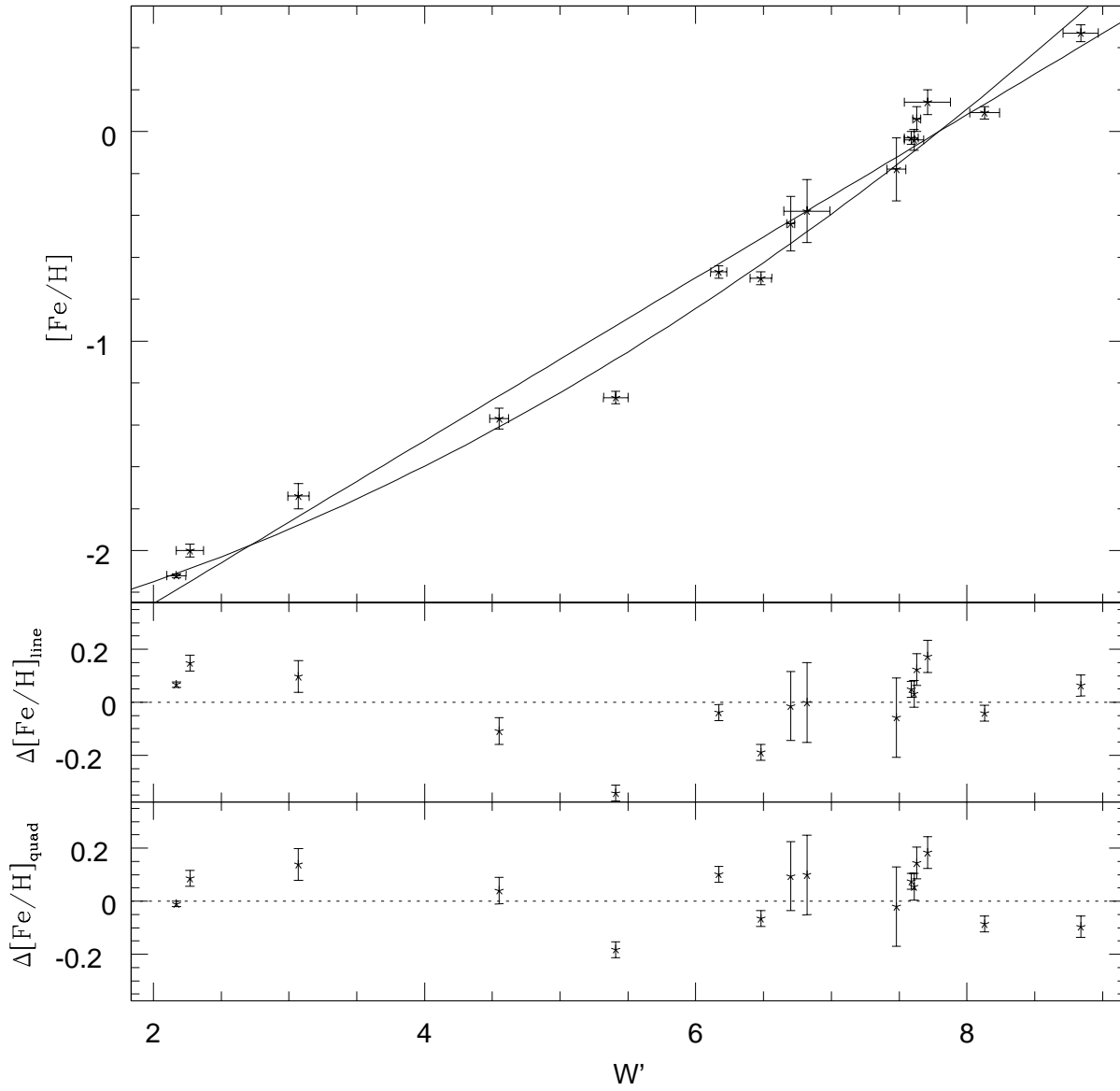


Figure 7. Top Panel: Calibration cluster metallicities from Table 8 plotted versus their W' values listed in Tables 6 and 7. The weighted (by metallicity) best fit line and parabola are also shown. Middle panel: Residuals to the best fit line with the 1σ reference metallicity errors shown. Bottom panel: Residuals to the best fit parabola with the 1σ reference metallicity errors shown.

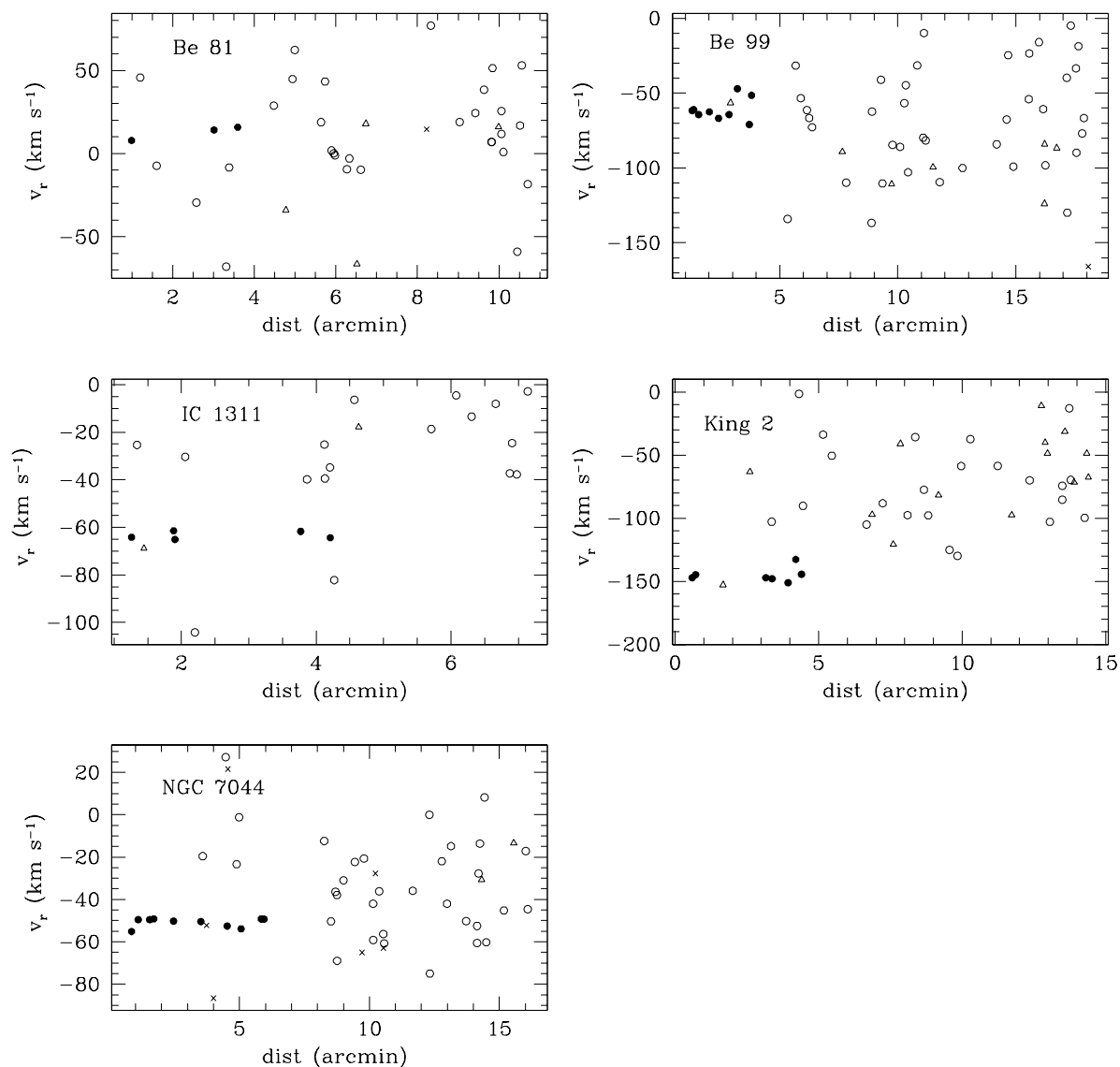


Figure 8. Accepted and rejected cluster members in our understudied clusters. Filled black circles are the accepted cluster stars based upon radial velocity and positional determinations. Open symbols are stars rejected from further analysis based upon radial velocities/falling beyond the visual cluster bounds (circles), TiO bands (crosses), CN bands (stars), and/or low quality spectra (triangles).

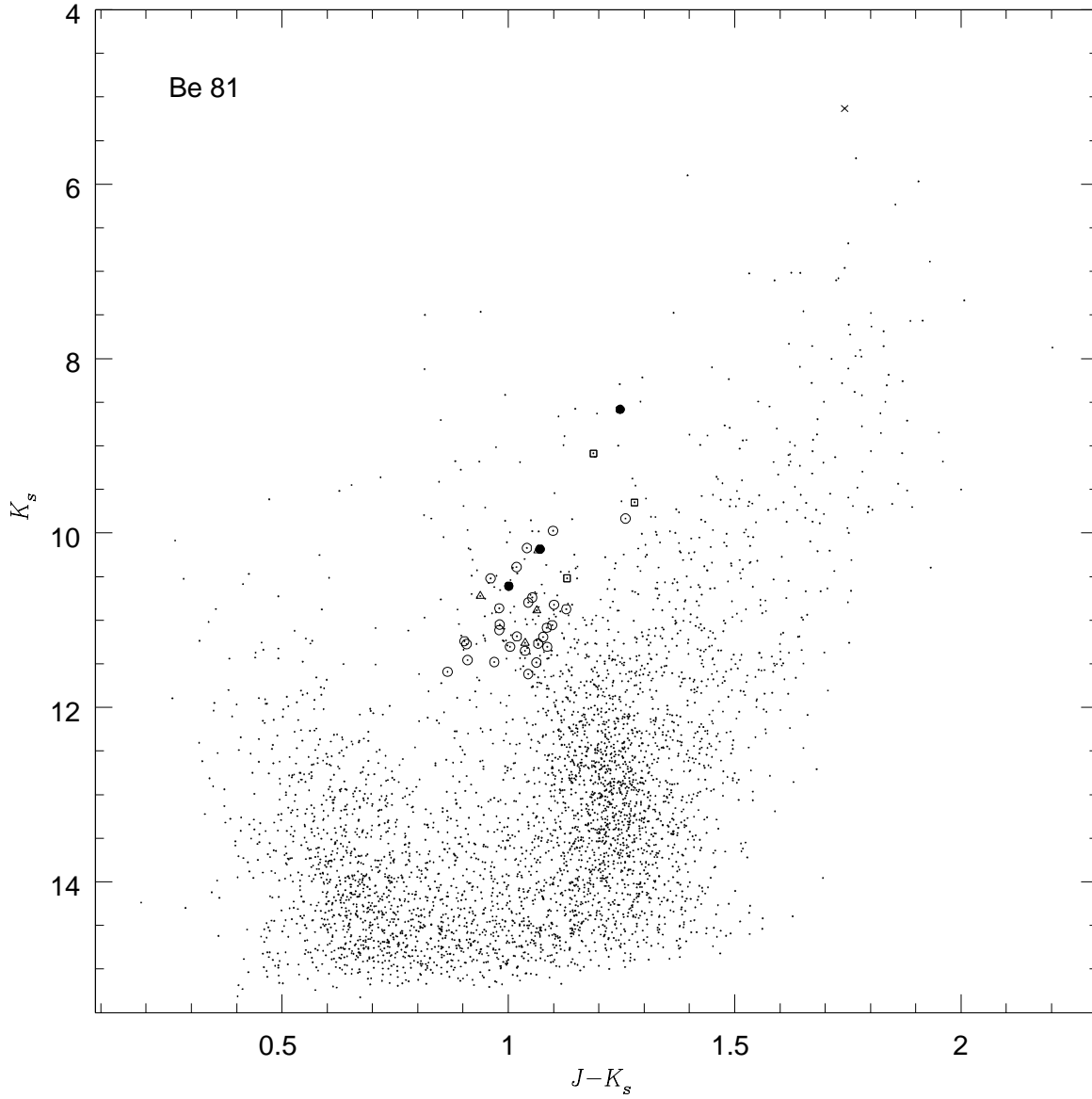


Figure 9. The 2MASS (K_s , $J - K_s$) CMD for Berkeley 81. Filled black circles are the accepted cluster stars based upon radial velocity and positional determinations. The open squares are part of the “fainter” subgroup and optical photometric outlier discussed in §3.1. Other open symbols are stars rejected from further analysis based upon radial velocities/falling beyond the visual cluster bounds (circles), TiO bands (crosses), CN bands (stars), and/or low quality spectra (triangles).

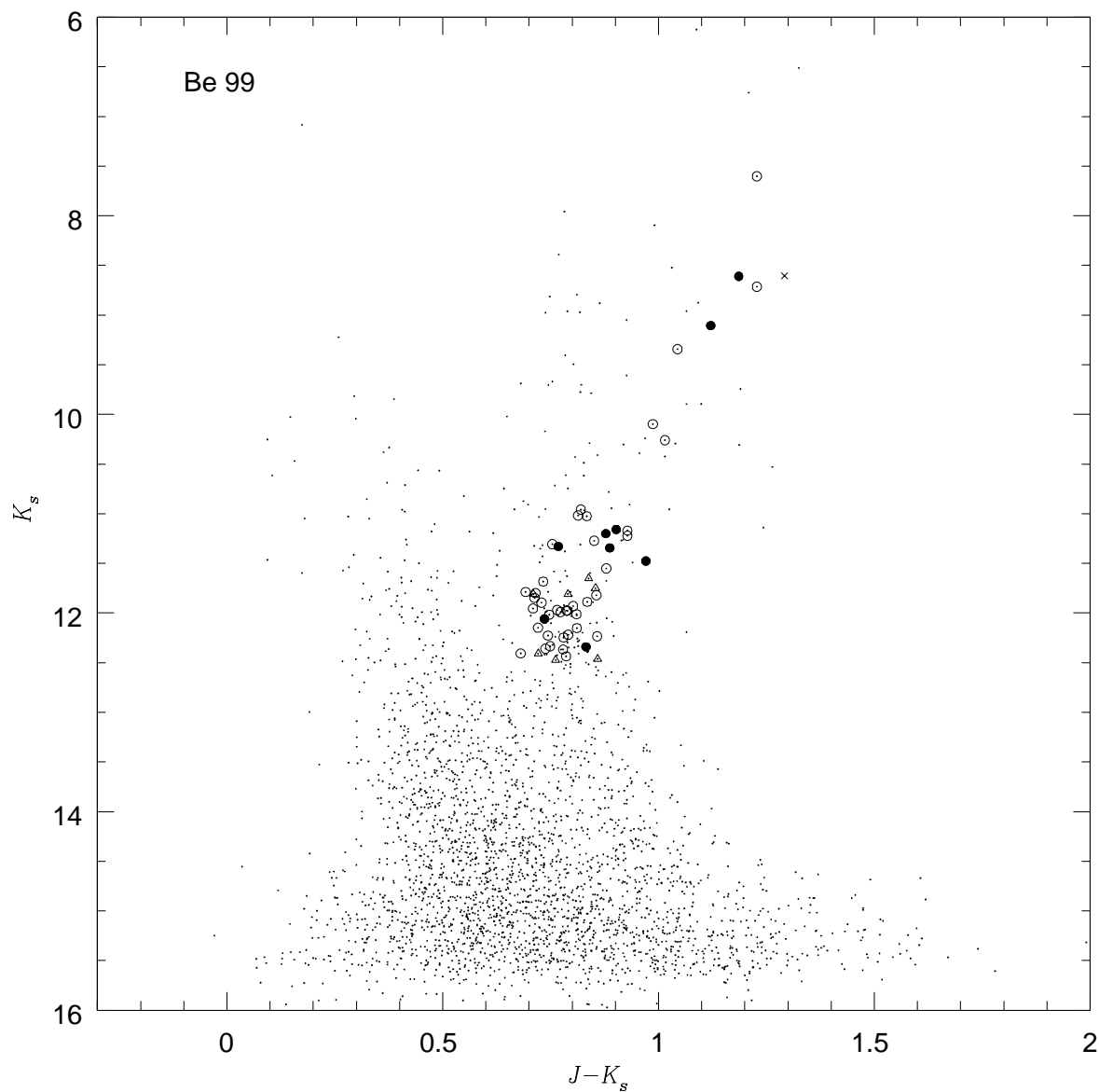


Figure 10. The 2MASS (K_s , $J-K_s$) CMD for Berkeley 99. Filled black circles are the accepted cluster stars based upon radial velocity and positional determinations. Open symbols are stars rejected from further analysis based upon radial velocities/falling beyond the visual cluster bounds (circles), TiO bands (crosses), CN bands (stars), and/or low quality spectra (triangles).

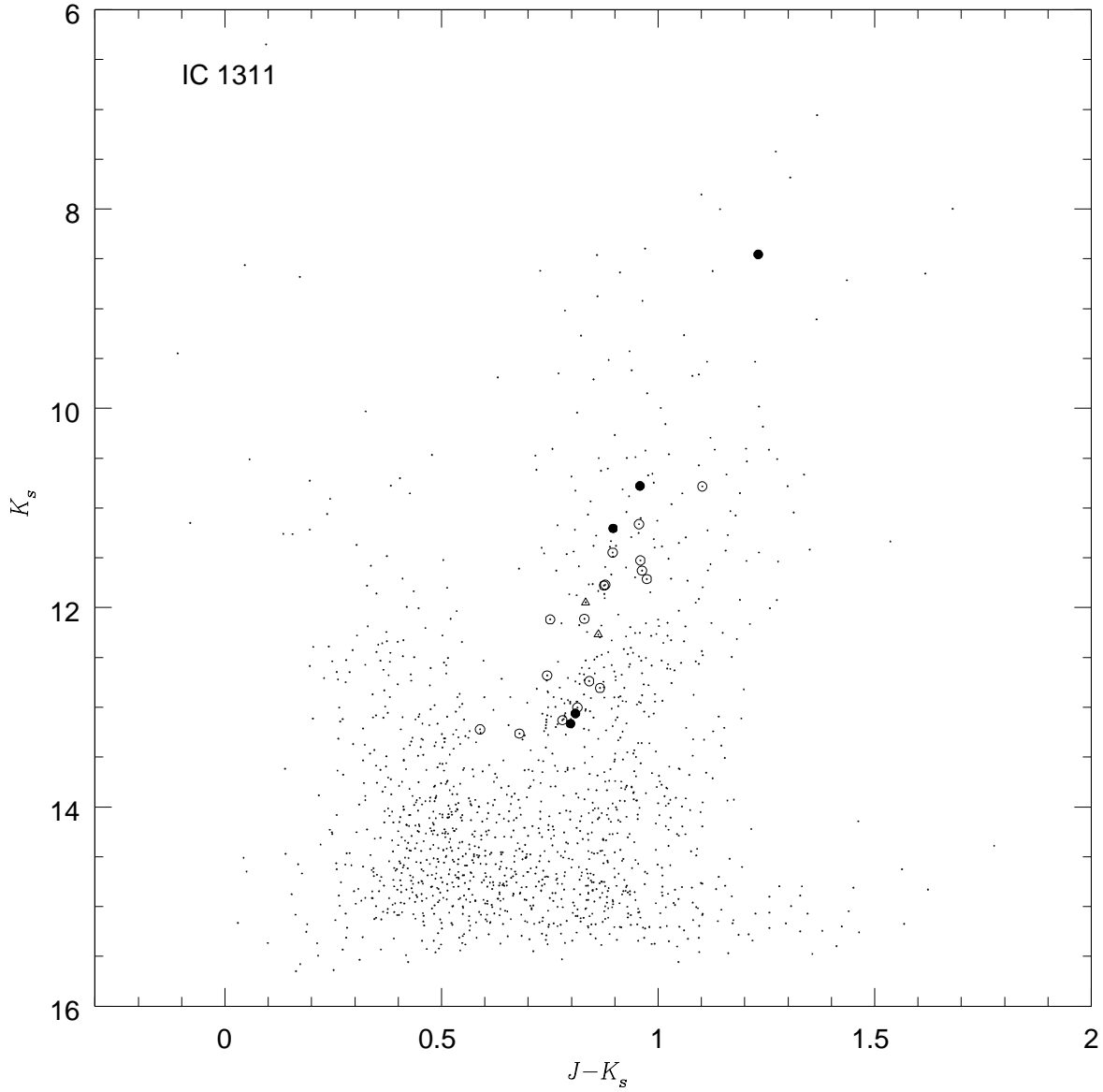


Figure 11. The 2MASS (K_s , $J - K_s$) CMD for IC 1311. Filled black circles are the accepted cluster stars based upon radial velocity and positional determinations. Open symbols are stars rejected from further analysis based upon radial velocities/falling beyond the visual cluster bounds (circles), TiO bands (crosses), CN bands (stars), and/or low quality spectra (triangles).

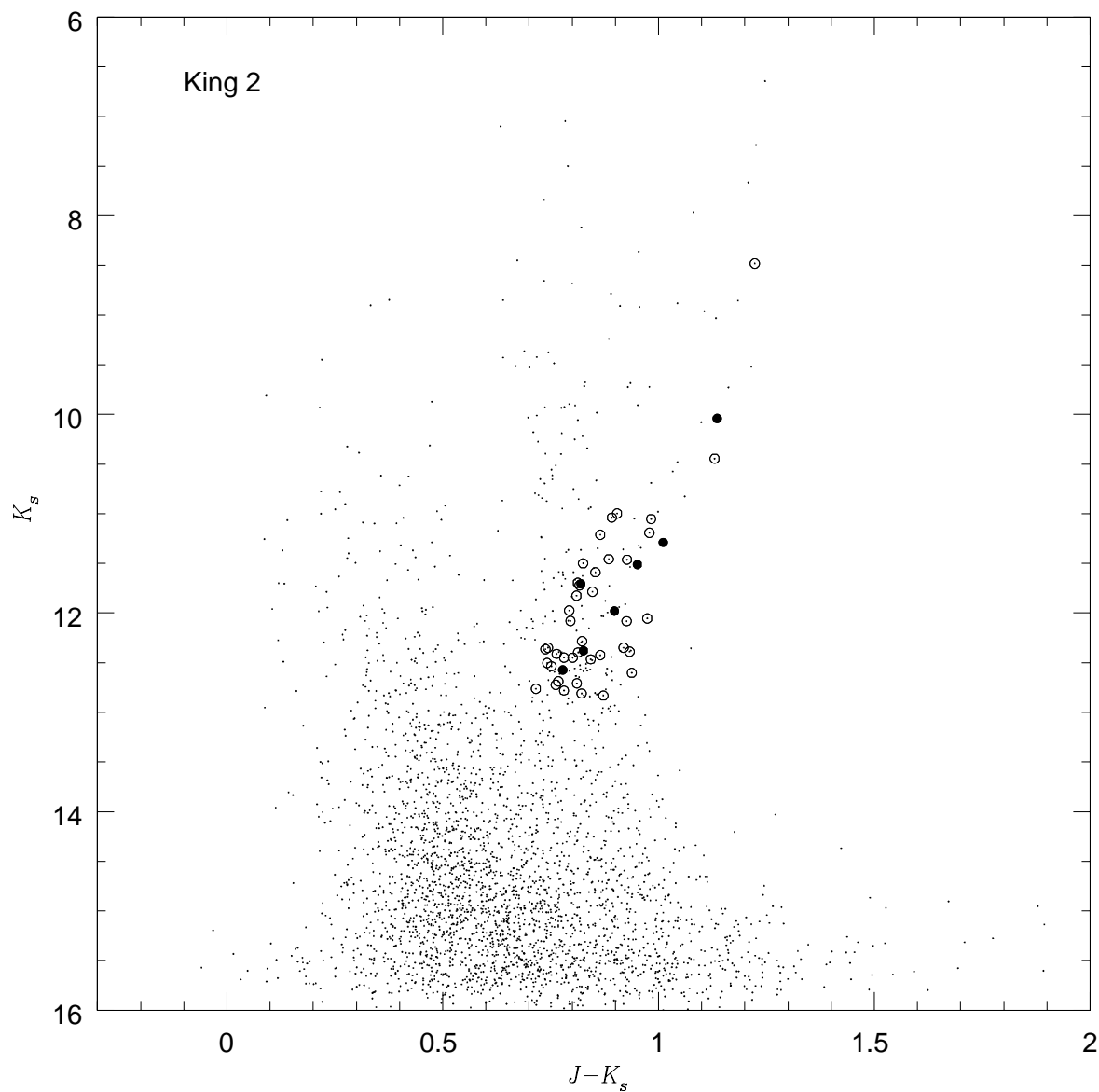


Figure 12. The 2MASS (K_s , $J - K_s$) CMD for King 2. Filled black circles are the accepted cluster stars based upon radial velocity and positional determinations. Open symbols are stars rejected from further analysis based upon radial velocities/falling beyond the visual cluster bounds (circles), TiO bands (crosses), CN bands (stars), and/or low quality spectra (triangles).

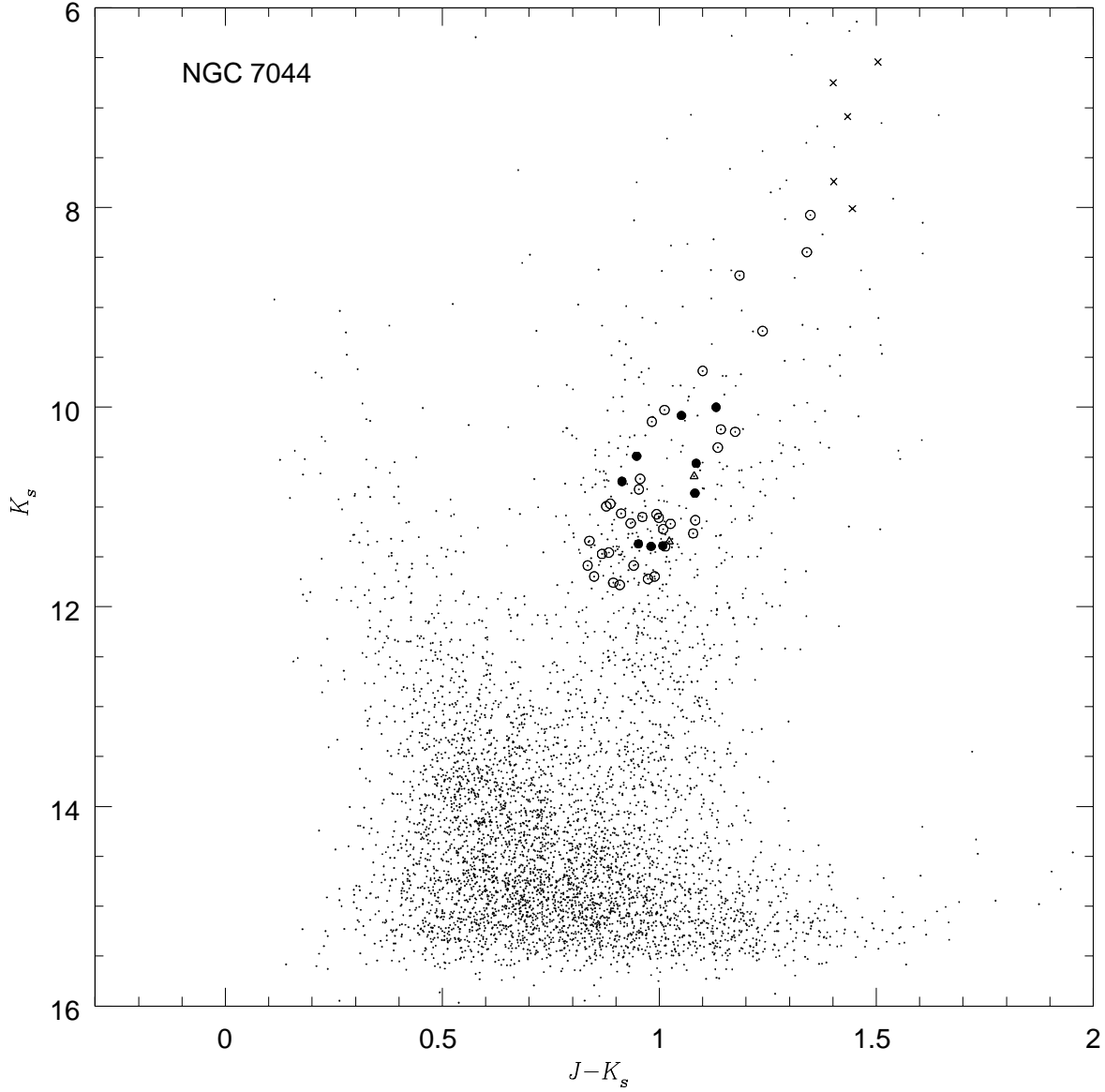


Figure 13. The 2MASS (K_s , $J-K_s$) CMD for NGC 7044. Filled black circles are the accepted cluster stars based upon radial velocity and positional determinations. Open symbols are stars rejected from further analysis based upon radial velocities/falling beyond the visual cluster bounds (circles), TiO bands (crosses), CN bands (stars), and/or low quality spectra (triangles).

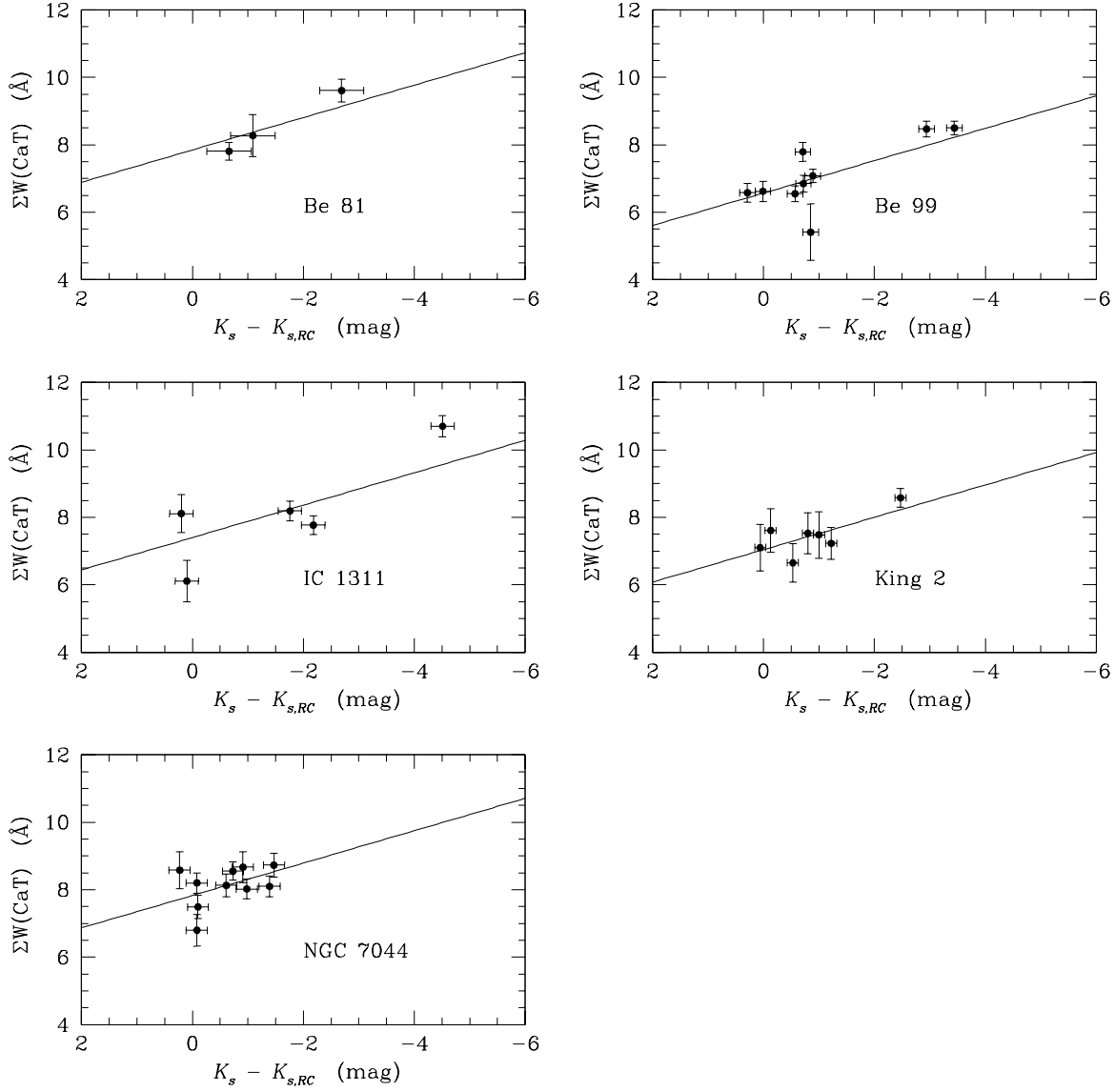


Figure 14. The best fit line using $\beta_{K_s} = 0.48$ as the slope for each cluster.